Research Square

Preprints are preliminary reports that have not undergone peer review.
They should not be considered conclusive, used to inform clinical practice,
or referenced by the media as validated information.

Annexin A2 plays a key role in protecting against acute kidney injury through β-catenin/TFEB pathway

Lili zhou (jinli730@smu.edu.cn)
Southern Medical University, Nanfang Hospital https://orcid.org/0000-0001-5044-6965

Kunyu Shen
Nanfang Hospital, Southern Medical University

Jinhua Miao
Southern Medical University, Nanfang Hospital

Qiongdan Gao
Southern Medical University, Nanfang Hospital

Xian Ling
Nanfang Hospital, Southern Medical University

Ye Liang
Nanfang Hospital, Southern Medical University

Qin Zhou
The Third Affiliated Hospital of Southern Medical University, Southern Medical University

Qirong Song
The Third Affiliated Hospital of Southern Medical University, Southern Medical University

Yuxin Luo
The Third Affiliated Hospital of Southern Medical University, Southern Medical University

Qinyu Wu
Southern Medical University, Nanfang Hospital

Weiwei Shen
Nanfang Hospital, Southern Medical University

Xiaonan Wang
Nanfang Hospital, Southern Medical University

Xiaolong Li
Nanfang Hospital, Southern Medical University

Youhua Liu
University of Pittsburgh

Shan Zhou
Southern Medical University, Nanfang Hospital

Ying Tang
The Third Affiliated Hospital of Southern Medical University, Southern Medical University

Article

Keywords: Annexin A2, Acute kidney injury, TFEB, Lysosome, Autophagy

Posted Date: July 8th, 2022

DOI: https://doi.org/10.21203/rs.3.rs-1358680/v1

License: This work is licensed under a Creative Commons Attribution 4.0 International License.
Read Full License

Version of Record: A version of this preprint was published at Cell Death Discovery on October 28th, 2022. See the published version at https://doi.org/10.1038/s41420-022-01224-w.

Abstract

Aim

Acute kidney injury (AKI) is becoming a heavy health burden worldwide. There are no effective therapeutic strategies nowadays. Recent studies showed that autophagy and lysosome stabilization could inhibit tubular cell apoptosis, and protect against AKI. Annexin A2 (ANXA2), a calcium-regulated phospholipid-binding protein, was found to be highly involved in autophagy. However, its role in AKI has not been elucidated.

Results

We found that ANXA2 is highly increased in renal tubular cells in cisplatin-treated mice, and in the urine and kidney samples from AKI patients. Ectopic expression of ANXA2 promoted lysosomal functions and autophagic flux, and protected against tubular cell apoptosis in AKI mice. Transcriptome analysis further identified that ANXA2 was intimately correlated with lysosome biogenesis, autophagy, and β-catenin signaling. Mechanistically, ANXA2 induced β-catenin activation through binding to and inhibiting on GSK3β, which further triggered T cell factor 4 (TCF4)-mediated transcription factor EB (TFEB) signaling pathway. As a result, TFEB activation regulated lysosomal proteostasis and effectively promoted autophagic flux. This greatly protected against renal tubular cell apoptosis and alleviated AKI.

Innovation:

These findings underline ANXA2 serves as a new therapeutic potential for AKI which lacks effective treatment.

Conclusion

We demonstrated that ANXA2 plays a key role in retarding AKI, which is associated with its inductive effects on β-catenin/TFEB-induced lysosmal pathway.

1 Introduction

Acute kidney injury (AKI), mainly caused by ischemic injury and toxicity (1), is primarily characterized by renal tubular epithelial cell injury (2). There is still no effective therapeutic strategy for AKI, which inevitably results in the progression into chronic kidney disease (CKD) (3). AKI has complex underlying mechanisms with multiple contributing factors. Of note, AKI is commonly occurred in hospitalized patients, especially in those who are subjected to ischemic injury and nephrotoxic drugs (3–6). Cisplatin is a commonly used chemotherapeutic agent, however, it has a high risk for triggering AKI (6, 7).

Therefore, a focus on specific drug-induced AKI may be necessary to understand the pathophysiology of AKI, and develop therapeutic strategies.

Autophagy is a series of self-defense process including phagophore, autophagosome and autolysosome formation, as well as cargo degradation and recycling, which helps to maintain physiological homeostasis (8). Recent studies found autophagy plays a key role in protecting against AKI (9, 10). Of interest, the effective dynamic process of membrane biogenesis and fusion plays an important role in inducing autophagy (11, 12). However, the inducer of this process in kidney injury still needs to be developed.

Annexin A2 (ANXA2), a 39-kDa phospholipid binding protein belonging to the Annexin family (13), plays a key role in the membrane-related organization, traffic and fusion processes (14, 15). Through assembling the interacting components at the membrane sites, ANXA2 is highly involved in dynamic events of membrane events (16, 17). Due to its ability to promote endocytosis and biological membranes to bind with each other, ANXA2 has been found to be a crucial mediator of autophagy (18, 19). ANXA2 gene deletion leads to phagophore defects for the lack of the essential components of membrane (20), and deficiency in autophagy (21). Interestingly, a previous report showed ANXA2 increases in AKI (22), however, the role of ANXA2 in AKI still remains unclear.

Wnt/β-catenin signaling is a developmental signal, but plays an important role in protecting against AKI (23). Upon Wnt stimulation, β-catenin translocates into nuclei to induce downstream targets through T cell factor (TCF)/ Lymphoid enhancer factor (LEF) family (24). Without Wnt signal, cytoplasmic β-catenin is commonly degraded by a destruction complex containing glycogen synthase kinase 3β (GSK3β) (25), suggesting that GSK3β is a key regulator of β-catenin degradation (26). Interestingly, ANXA2 is a modulator of GSK3β (27), and can activate β-catenin/TCF4 signals in cancer cells (28). This indicates that ANXA2 could regulate β-catenin signaling through GSK3β pathway in kidney injury. However, this needs to be demonstrated in detail.

In this study, we found that ANXA2 was increased in AKI and protected against cisplatin-induced kidney injury through promoting lysosomal functions and autophagy. ANXA2 activated β-catenin signaling through binding to and inhibiting on GSK3β. Innovatively, we identified that transcription factor EB (TFEB), a key transcription factor regulating lysosome stability, is a new downstream target of β-catenin. Our study provided an important clue to therapy for AKI.

2 Materials And Methods

2.1 Cell line

Human proximal tubular cell line (HK-2) was purchased from the Cell Bank of the Chinese Academy of Sciences (Shanghai, China). Cells were maintained in DMEM/F12 culture medium supplemented with 10% fetal bovine serum and 1% penicillin/streptomycin (Gibco, CA, USA). Nuclear and cytoplasmic fractions were separated using a commercial kit (KeyGEN BioTECH, KPG1100, Jiangsu, China).

2.2 Animal model

The animal experiments were approved by the Ethics Committee on Use and Care of Animals of Southern Medical University, Guangzhou China. Male C57BL/6 mice (8-week-old) were purchased from the Experimental Animal Center of Southern Medical University (Guangzhou, China). Mice were kept in a standard 12-hour light-dark cycle under the specific-pathogen-free condition and were allowed for free access to water and food. Mice were randomized into treatment and vehicle groups using the online "Research Randomizer" (https://www.randomizer.org). Between 5 and 8 mice were included in each group to meet the minimum sample size requirement to perform an Analysis of Variance (ANOVA) test. The overexpression or interference of ANXA2 was achieved by a hydrodynamics-based gene delivery approach (29). Briefly, either the ANXA2 overexpression or small hairpin RNA (shRNA) plasmid or the empty vector was administered by a single tail vein injection at a dosage of 1.25mg/kg body weight. 24 hours later, cisplatin (Selleckchem, S1166) was administrated by a single intraperitoneal injection at a dosage of 25mg/kg body weight. Mice were sacrificed 48 hours after cisplatin injection. Kidney tissues and serum samples were collected for the following assessment.

2.3 Serum test of creatinine and urea nitrogen

Serum concentrations of creatinine and urea nitrogen were assessed using an automatic chemistry analyzer (AU480, Chemistry Analyzer, Beckman coulter, Atlanta, USA).

2.4 Study participants

This study received ethics approval from the Ethics committee of the Third Affiliated Hospital of Southern Medical University. The participants who were diagnosed with AKI (age > 18) were enrolled. Exclusion criteria included a known treatment on AKI prior to hospitalization. The first morning spot urine samples were obtained from consented participants after hospitalization. Recruitment occurred between 23rd March 2021 and 10th January 2022. The control urine samples were donated by healthy volunteers. Given that this is a preliminary study to examine the potential association between serum creatinine and urinary ANXA2, no formal sample size calculation was undertaken. The demographic and clinical data are provided in Supplementary Table S1. We also analyzed ANXA2 expression in human kidney biopsies from patients with AKI. Non-neoplastic kidney tissues derived from patients who had renal carcinoma served as the control.

2.5 Plasmid and lentivirus construction

The control empty vector pcDNA3, the ANXA2 shRNA plasmid, the ANXA2 and TCF4 expression plasmids, the Renilla luciferase reporter plasmid and the pGL3-TFEB promoter plasmid were constructed by Genecreate Biological Engineering Co., Ltd. (Wuhan, China). All constructs were verified by DNA sequencing. Primers used for plasmid construction are available upon request. The RFP-GFP-LC3B lentivirus was purchased from HanBio Technology (HANBIO, HB-LP2100001, Shanghai, China).

2.6 Terminal deoxynucleotidyl transferase dUTP Nick-End labeling (TUNEL) assay

The TUNEL assay was carried out using the TUNEL apoptosis Assay Kit (Beyotime Institute of Biotechnology, C1086, China) according to the manufacturer's protocol. Briefly, 4% paraformaldehyde fixed cells were incubated with a mixed solution composed of terminal deoxynucleotidyl transferase (TdT) buffer, TdT enzyme and FITC. After being counter-stained with Hoechst 33258 (Beyotime Institute of Biotechnology, China), cells were captured by fluorescent microscopy (Leica TCS SP2 AOBS, Leica Microsystems, Cambridge, UK).

2.7 Flow cytometry analysis of apoptosis

HK-2 cells were harvested and stained with the PE Annexin V Apoptosis Detection Kit (BD, 559763, USA) according to the manual instruction. The stained cells were then subjected to analysis using the instrument BD LSR fortessa X-20 (USA) within 1 hour. Flow cytometry data were analyzed using FlowJo Software (version 10, Ashland).

2.8 Western blotting and immunoprecipitation

The total protein concentrations were measured using the BCA kit (BioVision K813-5000 Milpitas, CA). Equal amounts of protein (15–40 μg) were subjected to SDS-PAGE electrophoresis and then were electro-transferred to a 0.45μm polyvinylidene difluoride membrane (Merck Millipore Ltd, IPVH00010, Ireland). The membrane was blocked in skim milk, and incubated with primary antibodies overnight at 4^{o}C and secondary horseradish peroxidase-conjugated antibody for 1 hour at room temperature. Signals were developed with an ECL kit (Applygen, p1020, Beijing, China). For the Co-IP assay, 200μg of cellular protein was incubated with primary antibody (4^{o}C with rotation, overnight). The protein complex was precipitated using agarose beads (Santa Cruz biotechnology, sc-2003, USA). Antibodies applied in the study (Supplementary Table S2) and unedited Western blot photos (Supplementary original data) are provided in the supplementary documents.

2.9 Quantitative real-time-polymerase chain reaction (qrtPCR)

Total RNA was isolated using Trizol (Invitrogen, 15596-025) according to manufacturer's instructions. Every 1μg of RNA was reverse transcribed in a 20 μL system using HiScript III RT superMix (+ gDNA wiper) (vazyme™, R323-01). 2 μL of cDNA from various samples were amplified by qrtPCR with specific primers which have been listed in the supplementary Table S3. Relative gene expression was quantified using ChamQ SYBR qPCR Master Mix (High ROX Premixed) (vazyme™, Q341-02/03) on an ABI PRISM 7000 Sequence Detection System (Applied Biosystems, Foster City, CA).

2.10 Chromatin immunoprecipitation (ChIP)

ChIP assays were performed according to the protocol of SimpleChIP Plus Enzymatic Chromatin IP Kit (Magnetic Beads) (Cell Signaling TECHNOLOGY, 38191, USA). Relative antibodies and sequence of primers used for ChIP-PCR are described in the supplementary documents.

2.11 Luciferase analysis

HK-2 cells were transiently co-transfected with renilla luciferase, pGL3-TFEB promoter reporter plasmid, and ANXA2 or TCF4 expression plasmids by Lipofectamine 2000 (11668-019, Invitrogen, USA). Cells were harvested and assayed using the Dual-Luciferase Reporter Assay Systems (Dual-luciferase Report Assay System, E1910, Promega, USA).

2.12 Pathological and immunohistochemical staining

Paraffin-embedded kidney sections were stained using periodic acid-Schiff staining according to standard procedure. Immunohistochemical and immunofluorescent staining were performed in paraffin and frozen sections. The slides were then consecutively incubated with the primary antibody and the secondary antibody, after which the signal was amplified with the ABC kit (VECTA ABC Kit, Peroxidase, PK-6100, USA). Finally, the signal was developed using the AEC (VECTASTAIN Elite ABC Kit, Peroxidase PK-6100, USA) or the DAB kit (Vector Laboratories SK-4100, USA). For immunofluorescent staining, the fluorophore-conjugated secondary antibody was added on the primary antibody incubated slides for 1 hour at room temperature. Sections were then counter stained with DAPI, washed with TBST and mounted for observation under the confocal microscope (Leica Microsystems CMS GmbH, TCS SP8 X, Germany). Antibodies applied in the staining procedure mentioned above are described in the supplementary documents.

2.13 Transmission electron microscopy (TEM)

To assess the ultrastructure of organelles involved in autophagy. Kidney tissues or HK-2 cells were collected and fixed in 1.25% glutaraldehyde (0.1 mol/L) in phosphate buffer. Ultrathin sections (60 nm) were prepared by a routine procedure and were examined under an electron microscope (JEOL JEM-1010, Tokyo, Japan).

2.14 Detection of autophagic flux

HK-2 cells were transfected with RFP-GFP-LC3B lentivirus (HANBIO, HB-LP2100001, Shanghai, China), and then stimulated with or without human recombinant ANXA2 protein (2 μg/mL) with or without cisplatin (25 μg/mL) for 24 hours. Autophagosomes and autophagolysosomes were observed with confocal microscope (Leica Microsystems CMS GmbH, TCS SP8 X, Germany). The RFP-GFP-LC3B sensor

enables detection of neutral-pH LC3B-positive autophagosomes (green fluorescence) and acid-pH LC3B-positive autophagolysosomes (red fluorescence).

2.15 Detection of lysosome

Live cells were incubated with Lyso-tracker-red (50nmol/L, Beyotime, China, C1046) for 10 minutes and then counterstained with Hoechst 33432 (1μg/mL, Beyotime, China, C1042) before being observed using confocal microscope (Leica Microsystems CMS GmbH, TCS SP8 X, Germany).

2.16 RNA sequencing and bioinformatics analysis

RNA extraction, quality control and subsequent sequencing were performed by Applied Protein Technology (Shanghai, China). Briefly, qualified RNA samples were used for paired-end library construction using the ABclonal mRNA-seq Lib Prep Kit (ABclonal, China) following the manufacturer's instruction. Then, PCR products were purified (AMPure XP system) and library quality was assessed on an Agilent bioanalyzer 4150 system. Finally, sequencing was performed with an Illumina Novaseq 6000/MGISEQ-T7 instrument. The data generated from Illumina/BGI platform were used for bioinformatics analysis.

2.17 Quantifications of staining

Immunohistochemical, immunofluorescence were quantified at high-powered (x400, x1000) fields from randomly selected 5 fields each section. Quantification of positive staining was assessed two researchers who were blinded to the group allocation using a computer-aided technique (Image Pro Plus).

2.18 Statistical analysis

All of the data are expressed as the mean ± standard error of the mean (SEM). Statistical analysis was carried out using SPSS 20.0 (SPSS Inc, Chicago, IL). The Student's t test or t' test was used to compare the means between two groups. ANOVA was used to compare the means among three or more groups, followed by the Least Square Difference *post hoc* test when the variance between groups was homogeneous, or the Dunnett T3 test when the variance between groups was not homogeneous. A P value < 0.05 was considered to be statistically significant.

3 Results

3.1 Annnexin A2 is upregulated in AKI model

We first measured the gene expression levels of annexins family in the kidneys from normal mice and cisplatin-treated AKI mice. Notably, ANXA2 is the most significantly upregulated gene among the annexins gene family (annexins A1-13) (Fig. 1A). The increase in ANXA2 protein expression in cisplatin-injured kidney was also confirmed using western blotting (Fig. 1B and 1C). We next assessed the expression of ANXA2 in cisplatin-induced AKI mice model using immunofluorescent staining. The upregulation of ANXA2 in AKI was exhibited across different areas of cisplatin-injured kidney, including the cortex, cortex-medullar junction and medulla (Fig. 1D to G). We further performed co-staining of ANXA2 with different segment markers specifically indicating a certain type of tubular cell. As shown, ANXA2 was primarily co-localized with both proximal and distal renal tubule, and to a less extent, with collecting duct (Fig. 1H). We next quantified the concentration of ANXA2 in mouse urine using western blotting. As shown, urinary ANXA2 was strikingly increased in cisplatin-treated mice, indicating that ANXA2 may function as a biomarker for AKI (Fig. 1I and 1J).

3.2 ANXA2 is upregulated in human AKI

To test whether ANXA2 was also upregulated in the setting of human AKI, we measured urinary ANXA2 levels in AKI patients. Several urine samples were first analyzed using western blotting. As shown, compared to healthy controls, the urinary ANXA2 level was significantly increased in AKI patients (Fig. 2A and 2B). Urinary ANXA2 levels were further quantified using ELISA in a cohort of AKI patients. As shown in Fig. 2C, urinary ANXA2 was significantly upregulated in AKI. We next performed the immunohistochemical staining in AKI biopsy section. As shown in Fig. 2D, ANXA2 was upregulated in AKI-affected kidney, especially in tubules. We then performed correlation analysis of ANXA2 with serum creatinine. As shown in Fig. 2E, urinary ANXA2 were negatively associated with serum creatinine. This finding suggested ANXA2 might function as a protective biomarker in the progression of AKI.

3.3 ANXA2 protects against AKI

To explore whether ANXA2 plays a crucial role in protecting against AKI, we adopted cisplatin-induced AKI mouse model. Ectopic expression of ANXA2 was induced by injection of an expression plasmid (pCMV-ANXA2) through a hydrodynamic approach, which was commonly used to overexpress gene in kidneys as previously reported (29). The experimental design was shown in Fig. 3A. As shown in Fig. 3B, ANXA2 mRNA was increased in cisplatin-treated mice, but further elevated in ANXA2-overexpressed mice. Ectopic ANXA2 significantly inhibited tubular injury (Fig. 3C and 3I). The assessment of serum creatinine and urea nitrogen also revealed that ectopic ANXA2 effectively protected kidney function (Fig. 3D and 3E). We next measured the expression of apoptosis-related protein. Western blot results demonstrated that ectopic ANXA2 significantly decreased the expression of cleaved PARP-1 and caspase-3 (Fig. 3, F to H). Consistently, TUNEL staining also indicated that ectopic ANXA2 could significantly block cell apoptosis (Fig. 3I and 3J). The similar result was observed when Kim-1, a tubular cell injury marker, was examined by immunohistochemical staining (Fig. 3I and 3K). These results suggest that ANXA2 could protect against cell apoptosis in AKI.

3.4 ANXA2 protects against AKI and this is associated with its regulatory effects on autophagy, lysosomal functions, and Wnt/β-catenin signaling

To determine the underlying mechanisms, we performed RNA-sequencing using renal tissue sampled from the three groups of mice. The heatmap (Supplementary Fig S2A and Fig. 4A) demonstrated the gene expression profile among groups was significantly different in regulation of apoptosis, autophagy, lysosomal functions, and Wnt/β-catenin signaling. GSEA analysis was also performed to identify the above-mentioned pathways (Supplementary Figure S2C). As shown, RNA sequencing data strongly suggested that ANXA2 protected against AKI through those pathways.

We firstly checked the expression of β-catenin using immunohistochemical staining. As shown in Fig. 4B and C, the expression of β-catenin was suppressed in cisplatin-treated mice but restored by overexpression of ANXA2. The similar result was observed when β-catenin was examined by western blotting (Fig. 4D and E). We next assessed lysosomal functions. As shown in Fig. 4F and I, the protein expression of lysosome markers Lamp1, Lamp2 and TFEB, was downregulated in cisplatin-treated mice, but significantly preserved when ANXA2 was overexpressed. Consistently, the staining of TFEB and Lamp1 showed that they were decreased in cisplatin-treated mice, but greatly restored by ectopic expression of ANXA2 (Fig. 4, J to L). We next performed the qPCR analysis of multiple lysosome-related genes including TFEB, Lamp1, Lamp2, PSAP, TPP1, and atp6ap1. As shown in Fig. 4M, most of them were downregulated in cisplatin-treated mice, but significantly restored by co-treatment with ANXA2 overexpression. These results suggest that ANXA2 plays a key role in maintaining lysosomal functions, and the underlying mechanism is possibly associated with its inductive role in β-catenin pathway.

3.5 ANXA2 promotes lysosome-mediated autophagic flux function *in vivo*

To further explore the role of ANXA2 in lysosomal functions and autophagy, we first assessed the lysosome numbers in proximal tubular cells derived from three groups of mice by transmission electron microscope (TEM) analysis. As shown in Fig. 5A and B, the lysosme numbers were decreased in cisplatin-treated mice, but greatly restored in ANXA2-cotreated group. We then assessed the autophagy-related protein expression. As shown in Fig. 5C and D, western blotting analyses showed that ANXA2 significantly attenuated the expression of p-mTOR, and increased the expression of Atg5 and LC3BII (Fig. 5, C, E and F), suggesting the activated role of ANXA2 in autophagic pathway. We next performed the immunofluorescent staining of LC3B. As shown in Fig. 5G and H, ectopic ANXA2 greatly promoted the maturation of LC3B, as characterized by the assembly of positive puncta. We further observed the mitochondria and autophagosome and autolysosome formation using TEM. As shown in Fig. 5I and J, ectopic expression of ANXA2 could preserve the healthy mitochondria, and effectively trigger a series of processes of autophagic flux processes including autophagosome formation, antophagosome fusion

with lysosome, and lysosome-mediated degradation. These results further suggest that ANXA2 promotes lysosome-mediated autophagy function.

3.6 Knockdown of ANXA2 worsens AKI and apoptosis *in vivo*

We then knocked down gene expression of ANXA2 in cispaltin-treated mice (Fig. 6A). As shown in Fig. 6B, qPCR result showed that ANXA2 was increased in cisplaitn-treated mice, but successfully knocked down by shRNA injection. Scr and BUN levels were then assessed. As shown in Fig. 6, C and D, knockdown of ANXA2 could further aggravated the increase in Scr and BUN levels. We then analyzed tubular cell injury. PAS and Kim-1 staining were performed. As show in Fig. 6, E to G, cisplatin induced tubular cell injury, and this was further aggravated when ANXA2 was knocked down. We further measured the expression of apoptosis-related proteins including Fasl, Bax, and cleaved caspase 3. As shown in Fig. 6, H to K, all of them were upregulated in cisplatin-treated mice, and further increased when ANXA2 was interfered. TUNEL staining also revealed that interference of ANXA2 further induced cell apoptosis in cisplatin-treated mice (Fig. 6, L and M).

3.7 Knockdown of ANXA2 decreases lysosomal function and inhibited autophagy

We further assessed functions of lysosome and autophagy. TFEB and Lamp1 were firstly checked by immunostaining. As shown in Fig. 7, A to C, they were decreased by cisplatin injection, but further inhibited by knockdown of ANXA2. We next assessed TFEB and other genes related with lysosomal functions by qPCR. As shown in Fig. 7, D and E, most of them were decreased in cisplatin-treated mice, and further inhibited by ANXA2 interference. The similar results were observed when Lampl, Lamp2 and TFEB were assessed by western blotting (Fig. 7, F to I). Lysosome numbers were also tested by TEM. As shown in Fig. 7, J and K, knockdown of ANXA2 could further decreased lysosome numbers in cisplatin-treated mice. We next assessed autophagy-related proteins. As shown in Fig. 7, L to O, treatment with cisplatin increased p62, decreased Atg5, and LC3BII formation, and this was further aggravated when ANXA2 was knocked down.

3.8 ANXA2 blocks renal tubular cell apoptosis and promotes autophagy *in vitro*

We next explored the role of ANXA2 *in vitro*. HK-2 cells were co-treated with cisplatin (25 μg/mL, 24 h) and recombinant human ANXA2 protein (2 μg/mL). As shown in Fig. 8A, TUNEL staining assay revealed that ANXA2 evidently decreased apoptosis in cisplatin-treated cells. We next assessed the apoptotic rate by Annexin V staining using flow cytometry analysis (Fig. 8B). The results further confirmed that ANXA2 significantly inhibited cell apoptosis in renal tubular cells (Fig. 8C). Furthermore, the apoptosis-related proteins were tested by western blotting analyses. As shown in Fig. 8, D to G, co-treatment with ANXA2 could significantly inhibit cleaved PARP-1 and caspase-3 expression, and restored the expression of Bcl-2,

an anti-apoptotic protein. These results further demonstrated that ANXA2 inhibits renal tubular cell apoptosis.

We next assessed the effects of ANXA2 on authophagy. As shown in Fig. 8, H to K, co-treatment with ANXA2 could significantly inhibit the expression of p-mTOR and p62, and increased the expression of LC3BII in cisplatin-treated cells. We further assessed autophagic flux in HK-2 cells transfected with the lentiviral biosensor containing GFP-LC3B and RFP-LC3B. The RFP-GFP-LC3B sensor enables LC3B-positive, neutral-pH autophagosomes to emit green fluorescence, whereas LC3B-positive acidic pH autophagolysosomes to exhibit in red fluorescent color. As shown in Fig. 8L, ANXA2 overexpression induced autophagolysosome formation. The effects of ANXA2 in autophagic flux were also tested in cisplatin-treated cells. As shown in Fig. 8M and N, in cisplatin-treated cells, the fluorescent color of LC3B positive puncta was mostly green and yellow (overlap of red and green fluorescence), suggesting cisplatin induced autophagosome accumulation without fusion with lysosomes. However, a strong staining of RFP-LC3B positive puncta was observed in ANXA2 co-treated group, suggesting ANXA2 greatly triggered the autophagic flux. Of note, ICG-001, an inhibitor of β-catenin pathway, could block the inductive effects of ANXA2 in autophagic flux, suggesting the meditative role of β-catenin in ANXA2-activated autophagic flux.

3.9 ANXA2 promotes lysosomal functions through β-catenin/TCF4 signaling

We further assessed the lysosomal function in ANXA2-transfected cells. As shown in Fig. 9A, ANXA2 overexpression upregulated the gene expression of TFEB. Immunofluorescent staining demonstrated that ANXA2 induced the nuclear translocation of TFEB (Fig. 9B and C), an active form of TFEB. Other genes related with lysosomal function including Lamp1, Lamp2, PSAP, Atp6ap1 and TPP1, were also significantly induced by ANXA2 overexpression (Fig. 9D). Lysosomes were then labeled by lysosomal tracker staining (Fig. 9E). As shown in Fig. 9F, cisplatin treatment decreased lysosome numbers, and this was further aggravated by ANXA2 interference or inhibited by ANXA2 overexpression.

We next explored the relationship between ANXA2 and β-catenin pathway. A previous report showed that ANXA2 interacts with GSK3β in other organ (30). Hence, we tested whether ANXA2 could bind to GSK3β in renal tubular cells. Immunoprecipitation assay showed that ectopic expression of ANXA2 induced the binding of ANXA2 with GSK3β (Fig. 9G). Interestingly, we also found that ectopic expression of ANXA2 decreased mRNA and protein expression of GSK3β (Fig. 9, H and J). As an important component of destruction complex of β-catenin, GSK3β inhibition would lead to the activation of β-catenin. Therefore, we assessed the expression of nuclear β-catenin, an active form of it. As shown in Fig. 9I, ANXA2 overexpression induced the accumulation of β-catenin and its downstream transcription factor TCF4 in nuclear fraction. We also observed the nuclear TFEB expression in ANXA2-treated cells, suggesting the intimate relationship between TFEB and β-catenin/TCF4 pathway. We then performed the bioinformatics analysis, and found that there are TCF/LEF consensus core sequences in human, mouse, and rat TFEB gene promoter regions (Fig. 9K), suggesting the regulative role of β-catenin in TFEB. To testify the

hypothesis, we performed luciferase reporter assessment. As shown in Fig. 9L, overexpression of ANXA2 or TCF4 could significantly induce the transcriptional activity of TFEB. Furthermore, ChIP-PCR assay also confirmed the binding of TCF4 with TFEB promoter region (Fig. 9M). qPCR results also demonstrated that TCF4 overexpression increased TFEB mRNA expression (Fig. 9N). Furthermore, ANXA2-induced TFEB mRNA increase was further elevated by TCF4 overexpression or decreased by TCF4 interference (Fig. 9O).

We next examined the role of GSK3β/β-catenin/TCF4 pathway in modulating TFEB activity in cisplatin-treated cells. As shown in Fig. 9P, cisplatin-decreased TFEB mRNA level could be restored by ANXA2 overexpression, but this was inhibited by TWS119, a specific GSK3β inhibitor. Furthermore, cisplatin-decreased TFEB mRNA level could be preserved by overexpression of TCF4, or decreased by TCF4 interference (Fig. 9Q). These results further suggest that ANXA2 protected lysosomal function through β-catenin/TCF4/TFEB signaling.

3.10 Working model

The schematic diagram demonstrates that ANXA2 promotes lysosomal function to reinforce autophagic flux (Fig. 10). As shown, ANXA2 interacts with GSK3 β to inhibit its activity, which leads to β-catenin activation and tranlocation into nucleus to trigger TCF4-induced TFEB transcription. Furthermore, TFEB induces lysosome biogenesis and promotes lysosome-mediated autophagic flux, which inhibited cell apoptosis in renal tubular cells. Our results provided a potential therapeutic target for AKI.

4 Discussions

AKI is in high incidence nowadays, however, there are no effective therapeutic strategies. Autophagy and lysosomal functions are highly related with the progression of AKI. However, their modulators still need to be investigated in detail. With dynamic processes of membrane biogenesis, fusion and separation, autophagy and lysosomal functions were strongly affected by some regulating factors such as the Annexin family (14, 15). Interestingly, a previous report showed ANXA2 increases in AKI (22), however, the role of ANXA2 in AKI remains unclear.

Previous reports showed that ANXA2 is related with AKI (22, 31), however, the authentic role of ANXA2 in AKI remains poorly understood. We found that ANXA2 plays a key role in protecting against AKI through inducing autophagy and lysosomal function, and the related mechanism is highly associated with β-catenin. To the best of our knowledge, our study for the first time addressed the meditative role of ANXA2 in autophagy under the condition of AKI.

Autophagy defects in renal tubular epithelial cells are closely associated with AKI progression (32). Autophagy is highly dependent on the functional stability and structural integrity of the organelle membrane (33). Of note, ANXA2 plays a key role in regulating biological membranes (16) and autophagy (21) in other organs. However, its role and underlying mechanisms in AKI are not elucidated. Herein, we observed ANXA2 contributes to the integrity of the autophagosome membrane and the fusion of autophagosome with lysosome. Then, ANXA2 promotes lysosomal biogenesis and increases lysosomal

functions in tubular cells. These suggest that ANXA2 could trigger another signaling pathway beyond membrane organization. Interestingly, we found β-catenin/TFEB pathway is highly involved.

Previous researches showed that lysosome plays a protective role in autophagic processes in AKI (34). TFEB is crucial transcription factor in regulating kidney injury through inducing lysosome biogenesis and functions (35, 36). *In vivo*, we delivered ANXA2 expression or interference plasmids through a dynamic approach, the gene delivery to kidney effectiveness of which has been reported previously (29, 37). We also observed the overexpression or interference of ANXA2 (Figs. 3 and 6), which suggested the sufficient efficiency of plasmid uptake from the circulation. We could not exclude the non-renal effects of ANXA2 overexpression or interference as the plasmids were delivered through the circulation, especially when considering ANXA2 also has a role in regulating immune-response and inflammation (38). Indeed, we also observed the interstitial expression of ANXA2 in AKI, which is maybe at the location of some immune cells. However, this is beyond the scope of this study and needs to be further investigated in detail in the future. Of note, we found that ANXA2 was primarily increased in tubules from AKI-affected kidneys, and promoted autophagy and lysosomal functions. This suggested that tubular cell-derived ANXA2 was the main functional factor for beneficial effects in AKI.

Furthermore, we found that ANXA2 overexpression could greatly promote lysosomal functions and autophagy, restore the expression of TFEB, and lead to the activation of Wnt/β-catenin signaling, suggesting the intimate correlation among them. Interestingly, we found that ANXA2 induces β-catenin signaling activation through GSK3β, which further triggers TFEB-mediated lysosomal biogenesis. Of note, TFEB subcellular localization could be modulated by its phosphorylation status (39). It would be best to identify the phosphorylation status of TFEB induced by ANXA2, however, this is beyond the scope of this study. Instead, we have observed that ANXA2 induced the nuclear translocation of TFEB, which also represents the activation of TFEB (39). An important finding in this study was that TFEB is a new downstream target of β-catenin. This was first recognized in our study, which may explain the underlying mechanisms of β-catenin in protecting against AKI.

Interestingly, we found that ANXA2 was increased in AKI experimental models and human biopsy, however, it was negatively correlated with levels of serum creatinine. As renal tubular epithelial cells have a strong capability of self-repair, hence, upon slight and mild insults, some tubular cells would undergo regeneration through producing ANXA2. We therefore reckoning ANXA2 represented a compensatory mechanism for tubular cell repair and regeneration. Indeed, we have observed that ANXA2 strongly protected against tubular cell apoptosis and kidney injury through β-catenin signaling. This is consistent with the previous observations, i.e., β-catenin and its downstream target MMP-7 were both increased in AKI and they inhibited the progression of AKI (40–42). The expression and role of MMP-7 in AKI could also help explain why ANXA2 exerted inhibitory effects on AKI progression.

In animal experiments, we adopted cisplatin-induced mice models for its superiority in study on autophagy and lysosomal functions in AKI (43, 44). We admit that cisplatin stimulation could induce a transient enhancement of autophagy and lysosomal functions (43), however, it damaged autophagy,

decreased TFEB expression and lysosomal functions with a long-term exposure in the kidney (44, 45). Hence, this model has advantage in research on specific drugs which could affect AKI progression through modulating autophagy and lysosomal functions. In this model, we found that cisplatin triggered TFEB and autophagy inhibition, although ANXA2 was concomitantly increased. This further indicated that upregulation of ANXA2 is a compensatory mechanism for AKI repair. However, under a long-lasting stimulus, the increased ANXA2 would finally not be enough to compensate the kidney injury. Consistently, we observed that urinary ANXA2 was negatively associated with serum creatinine, further suggesting the protective role of ANXA2 in renal function.

In this clinical cohort, we collected the the urine samples from hospitalized participants with AKI. Although the ischemic injury is the main cause for AKI initiation, the nephrotoxic drug-induced AKI still could not be ignored. Considering the etiological diversity of AKI, it will be important in future studies to explore the role of ANXA2 in AKI using a series of other animal models (e.g., the mouse model of renal ischemia-reperfusion injury). Additionally, though our study provided valuable insights regarding the diagnostic potential of ANXA2 in AKI, its clinical relevance is warranted to be thoroughly examined in a larger cohort.

Overall, we found a novel candidate, ANXA2, for addressing the increasing global concern in treatment for AKI. We also clearly elucidated that the underlying mechanism lied in the β-catenin/TFEB-triggered lysosomal functions. Although more studies are needed, our results demonstrated proof of principle that ANXA2 could serve as a new therapeutic target and a potential diagnostic biomarker for AKI. Our study also provided a new clue to better modulate AKI via reasonably enhancing lysosomal functions, which has rarely been investigated previously.

Declarations

ACKNOWLEDGEMENT

This work was supported by National Key R&D Program of China (2020YFC2005000); National Natural Science Foundation of China (Grant No. 82070707, 82070709, 91949114, 82100786, 82000652); Natural Science Foundation of Guangdong Province (Grant No. 2019A1515012197); Postdoctoral Science Foundation of China Grant (Grant No. 2021M701602, 2021M701636); Foundation of Chinese Project of Innovation Team of Chronic Kidney Disease with Integrated Traditional Chinese and Western Medicine (Grant No. 2019KCXTD014); Frontier Research Program of Guangzhou Regenerative Medicine and Health Guangdong Laboratory (Grant No. 2018GZR110105004); Outstanding Scholar Program of Guangzhou Regenerative Medicine and Health Guangdong Laboratory (Grant No. G2018GZR110102004); Outstanding youth cultivation program in Nanfang Hospital (Grant No. 2021J001); Presidential Foundation of Nanfang Hospital (Grant No. 2019Z006, 2019C026, 2021C023).

CONFLICT OF INTEREST

The authors declare no competing interest.

ETHICS STATEMENT

The animal experiments were approved by the Ethics Committee on Use and Care of Animals of Southern Medical University, Guangzhou China. The human study received ethics approval from the Ethics committee of the Third Affiliated Hospital of Southern Medical University.

DATA AVAILABILITY STATEMENT

Sequencing data produced in this study have been uploaded to the NCBI SRA database (accession number: PRJNA806160). Full unedited gels and blots produced in this study have been provide in the Supplementary material. Other raw data supporting the conclusion of this article will be made available by the authors, without undue reservation, to any qualified researcher.

AUTHOR CONTRIBUTIONS

Conceptualization, Lili Zhou; Project administration, Kunyu Shen and Jinhua Miao; Clinical sample and participant information collection, Ying Tang, Qin Zhou, Qirong Song and Yuxin Luo; Data analysis, Lili Zhou, Shan Zhou, Xian Ling, Ye Liang and Kunyu Shen; Results validation, all authors; Writing-review&editing, Lili Zhou, Shanzhou, and Kunyu Shen.

References

1. Vijayan A. Tackling AKI: prevention, timing of dialysis and follow-up. Nature reviews Nephrology. 2021;17(2):87–8.
2. Zuk A, Bonventre JV. Acute Kidney Injury. Annual review of medicine. 2016;67:293–307.
3. Li Q, Lin M, Huang H, Liu L, Chen W, Huang D, et al. Prevalence and mortality of transient acute kidney injury within 48 h, as new subtype, following coronary angiography: a cohort study. Clinical and experimental nephrology. 2022.
4. Thielmann M, Corteville D, Szabo G, Swaminathan M, Lamy A, Lehner LJ, et al. Teprasiran, a Small Interfering RNA, for the Prevention of Acute Kidney Injury in High-Risk Patients Undergoing Cardiac Surgery: A Randomized Clinical Study. Circulation. 2021;144(14):1133–44.
5. Parikh CR, Liu C, Mor MK, Palevsky PM, Kaufman JS, Thiessen Philbrook H, et al. Kidney Biomarkers of Injury and Repair as Predictors of Contrast-Associated AKI: A Substudy of the PRESERVE Trial. American journal of kidney diseases: the official journal of the National Kidney Foundation. 2020;75(2):187–94.
6. Chen KL, Shamavonian R, Karpes JB, Alzahrani NA, Morris DL. Acute Kidney Injury Following Hyperthermic Intraperitoneal Chemotherapy With Cisplatin. Anticancer research. 2021;41(3):1641–6.
7. Suppadungsuk S, Phitakwatchara W, Reungwetwattana T, Pathumarak A, Phakdeekitcharoen B, Kitiyakara C, et al. Preloading magnesium attenuates cisplatin-associated nephrotoxicity: pilot randomized controlled trial (PRAGMATIC study). ESMO open. 2021;7(1):100351.

8. Galluzzi L, Green DR. Autophagy-Independent Functions of the Autophagy Machinery. Cell. 2019;177(7):1682–99.
9. Minami S, Nakamura S. Therapeutic potential of Beclin1 for transition from AKI to CKD: autophagy-dependent and autophagy-independent functions. Kidney international. 2022;101(1):13–5.
10. Shen W, Jia N, Miao J, Chen S, Zhou S, Meng P, et al. Penicilliumin B Protects against Cisplatin-Induced Renal Tubular Cell Apoptosis through Activation of AMPK-Induced Autophagy and Mitochondrial Biogenesis. Kidney diseases. 2021;7(4):278–92.
11. Tanaka T, Warner BM, Michael DG, Nakamura H, Odani T, Yin H, et al. LAMP3 inhibits autophagy and contributes to cell death by lysosomal membrane permeabilization. Autophagy. 2021:1–19.
12. Barz S, Kriegenburg F, Sanchez-Martin P, Kraft C. Small but mighty: Atg8s and Rabs in membrane dynamics during autophagy. Biochimica et biophysica acta Molecular cell research. 2021;1868(9):119064.
13. Xi Y, Ju R, Wang Y. Roles of Annexin A protein family in autophagy regulation and therapy. Biomedicine & pharmacotherapy = Biomedecine & pharmacotherapie. 2020;130:110591.
14. Lopez-Rodriguez JC, Martinez-Carmona FJ, Rodriguez-Crespo I, Lizarbe MA, Turnay J. Molecular dissection of the membrane aggregation mechanisms induced by monomeric annexin A2. Biochimica et biophysica acta Molecular cell research. 2018;1865(6):863–73.
15. Berg Klenow M, Iversen C, Wendelboe Lund F, Mularski A, Busk Heitmann AS, Dias C, et al. Annexins A1 and A2 Accumulate and Are Immobilized at Cross-Linked Membrane-Membrane Interfaces. Biochemistry. 2021;60(16):1248–59.
16. Varyukhina S, Lamaziere A, Delaunay JL, de Wreede A, Ayala-Sanmartin J. The Ca(2+)- and phospholipid-binding protein Annexin A2 is able to increase and decrease plasma membrane order. Biochimica et biophysica acta Biomembranes. 2022;1864(1):183810.
17. Matos ALL, Grill D, Kudruk S, Heitzig N, Galla HJ, Gerke V, et al. Dissipative Microgravimetry to Study the Binding Dynamics of the Phospholipid Binding Protein Annexin A2 to Solid-supported Lipid Bilayers Using a Quartz Resonator. Journal of visualized experiments: JoVE. 2018(141).
18. Moreau K, Ghislat G, Hochfeld W, Renna M, Zavodszky E, Runwal G, et al. Transcriptional regulation of Annexin A2 promotes starvation-induced autophagy. Nature communications. 2015;6:8045.
19. Zhang HT, Zeng Q, Wu B, Lu J, Tong KL, Lin J, et al. TRIM21-regulated Annexin A2 plasma membrane trafficking facilitates osteosarcoma cell differentiation through the TFEB-mediated autophagy. Cell death & disease. 2021;12(1):21.
20. Morozova K, Sridhar S, Zolla V, Clement CC, Scharf B, Verzani Z, et al. Annexin A2 promotes phagophore assembly by enhancing Atg16L(+) vesicle biogenesis and homotypic fusion. Nature communications. 2015;6:5856.
21. Wang K, Zhang T, Lei Y, Li X, Jiang J, Lan J, et al. Identification of ANXA2 (annexin A2) as a specific bleomycin target to induce pulmonary fibrosis by impeding TFEB-mediated autophagic flux. Autophagy. 2018;14(2):269–82.

22. Cheng CW, Rifai A, Ka SM, Shui HA, Lin YF, Lee WH, et al. Calcium-binding proteins annexin A2 and S100A6 are sensors of tubular injury and recovery in acute renal failure. Kidney international. 2005;68(6):2694–703.
23. Schunk SJ, Floege J, Fliser D, Speer T. WNT-beta-catenin signalling - a versatile player in kidney injury and repair. Nature reviews Nephrology. 2021;17(3):172–84.
24. Liu J, Xiao Q, Xiao J, Niu C, Li Y, Zhang X, et al. Wnt/beta-catenin signalling: function, biological mechanisms, and therapeutic opportunities. Signal transduction and targeted therapy. 2022;7(1):3.
25. Albrecht LV, Tejeda-Munoz N, De Robertis EM. Cell Biology of Canonical Wnt Signaling. Annual review of cell and developmental biology. 2021;37:369–89.
26. Liu Q, Kong Y, Guo X, Liang B, Xie H, Hu S, et al. GSK-3beta inhibitor TDZD-8 prevents reduction of aquaporin-1 expression via activating autophagy under renal ischemia reperfusion injury. FASEB journal: official publication of the Federation of American Societies for Experimental Biology. 2021;35(8):e21809.
27. Pan H, Song Y, Zhang H, Bai Y, Konishi T, Kobayashi A, et al. Radiation engenders converse migration and invasion in colorectal cancer cells through opposite modulation of ANXA2/AKT/GSK3beta pathway. American journal of cancer research. 2021;11(1):61–78.
28. Tang T, Guo C, Xia T, Zhang R, Zen K, Pan Y, et al. LncCCAT1 Promotes Breast Cancer Stem Cell Function through Activating WNT/beta-catenin Signaling. Theranostics. 2019;9(24):7384–402.
29. Zhou S, Wu Q, Lin X, Ling X, Miao J, Liu X, et al. Cannabinoid receptor type 2 promotes kidney fibrosis through orchestrating beta-catenin signaling. Kidney international. 2021;99(2):364–81.
30. He X, Li X, Han Y, Chen G, Xu T, Cai D, et al. CircRNA Chordc1 protects mice from abdominal aortic aneurysm by contributing to the phenotype and growth of vascular smooth muscle cells. Molecular therapy Nucleic acids. 2022;27:81–98.
31. An L, Ji D, Hu W, Wang J, Jin X, Qu Y, et al. Interference of Hsa_circ_0003928 Alleviates High Glucose-Induced Cell Apoptosis and Inflammation in HK-2 Cells via miR-151-3p/Anxa2. Diabetes, metabolic syndrome and obesity: targets and therapy. 2020;13:3157–68.
32. Kaushal GP, Shah SV. Autophagy in acute kidney injury. Kidney international. 2016;89(4):779–91.
33. Soreng K, Neufeld TP, Simonsen A. Membrane Trafficking in Autophagy. International review of cell and molecular biology. 2018;336:1–92.
34. Zhang W, Li X, Wang S, Chen Y, Liu H. Regulation of TFEB activity and its potential as a therapeutic target against kidney diseases. Cell death discovery. 2020;6:32.
35. Liu X, Zheng X, Lu Y, Chen Q, Zheng J, Zhou H. TFEB Dependent Autophagy-Lysosomal Pathway: An Emerging Pharmacological Target in Sepsis. Frontiers in pharmacology. 2021;12:794298.
36. Nakamura S, Shigeyama S, Minami S, Shima T, Akayama S, Matsuda T, et al. LC3 lipidation is essential for TFEB activation during the lysosomal damage response to kidney injury. Nature cell biology. 2020;22(10):1252–63.

37. Zhou L, Chen X, Lu M, Wu Q, Yuan Q, Hu C, et al. Wnt/beta-catenin links oxidative stress to podocyte injury and proteinuria. Kidney international. 2019;95(4):830–45.
38. Dallacasagrande V, Hajjar KA. Annexin A2 in Inflammation and Host Defense. Cells. 2020;9(6).
39. Napolitano G, Esposito A, Choi H, Matarese M, Benedetti V, Di Malta C, et al. mTOR-dependent phosphorylation controls TFEB nuclear export. Nature communications. 2018;9(1):3312.
40. Fu H, Zhou D, Zhu H, Liao J, Lin L, Hong X, et al. Matrix metalloproteinase-7 protects against acute kidney injury by priming renal tubules for survival and regeneration. Kidney international. 2019;95(5):1167–80.
41. He W, Tan RJ, Li Y, Wang D, Nie J, Hou FF, et al. Matrix metalloproteinase-7 as a surrogate marker predicts renal Wnt/beta-catenin activity in CKD. Journal of the American Society of Nephrology: JASN. 2012;23(2):294–304.
42. Zhou D, Li Y, Lin L, Zhou L, Igarashi P, Liu Y. Tubule-specific ablation of endogenous beta-catenin aggravates acute kidney injury in mice. Kidney international. 2012;82(5):537–47.
43. Kaushal GP, Kaushal V, Herzog C, Yang C. Autophagy delays apoptosis in renal tubular epithelial cells in cisplatin cytotoxicity. Autophagy. 2008;4(5):710–2.
44. Zhu L, Yuan Y, Yuan L, Li L, Liu F, Liu J, et al. Activation of TFEB-mediated autophagy by trehalose attenuates mitochondrial dysfunction in cisplatin-induced acute kidney injury. Theranostics. 2020;10(13):5829–44.
45. Periyasamy-Thandavan S, Jiang M, Wei Q, Smith R, Yin XM, Dong Z. Autophagy is cytoprotective during cisplatin injury of renal proximal tubular cells. Kidney international. 2008;74(5):631–40.

Figures

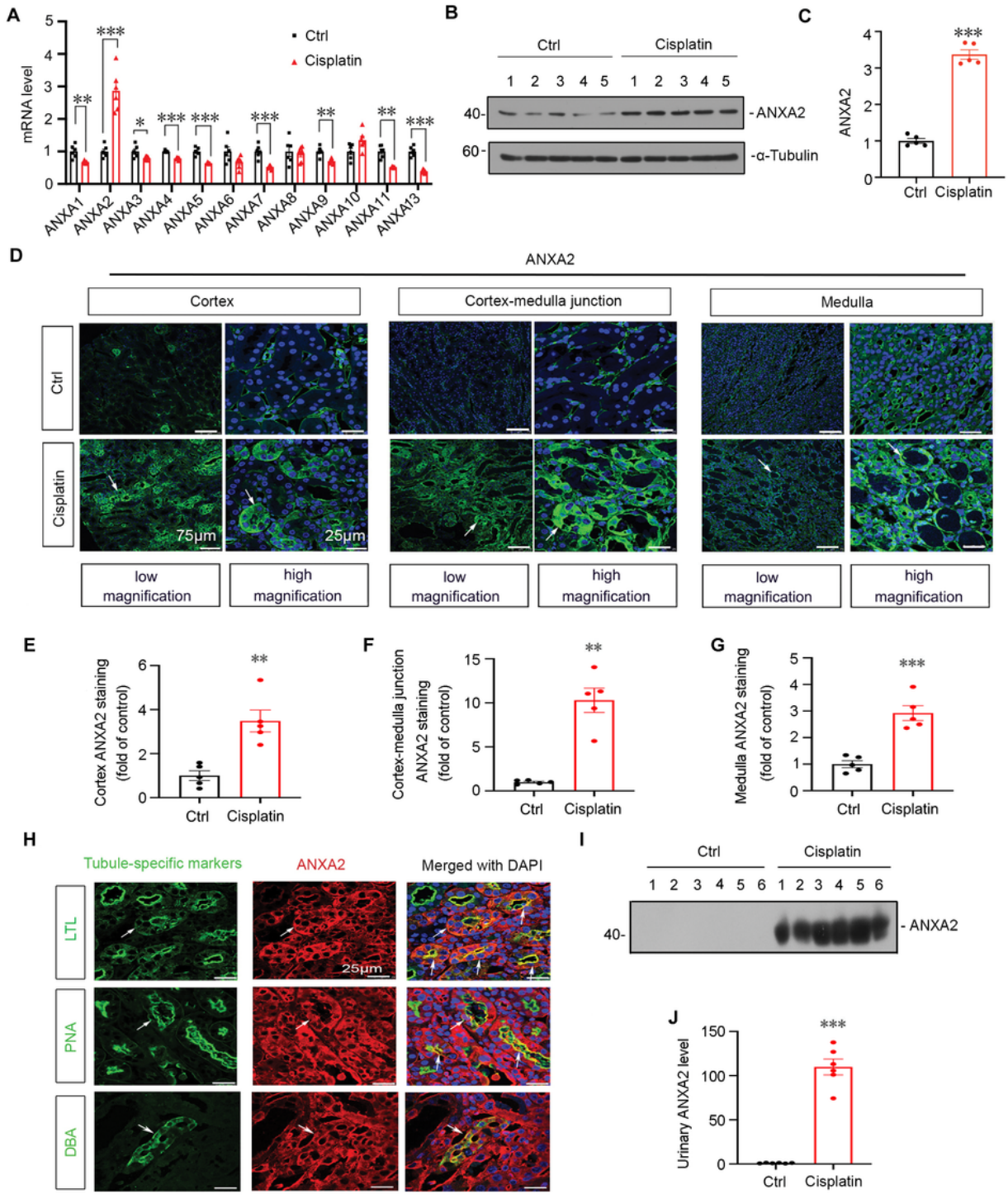

Figure 1

Figure 1

Annexin A2 is upregulated in AKI model

(A) Quantitative data show that among annexin gene family (Anxa1-13), mRNA level of ANXA2 is significantly higher in injured kidney versus the control kidney. Mean±SEM.*P<0.05,**P<0.01,***P<0.001, Cisplatin (n=6) versus Ctrl group (n=6). **(**B, C**)** Western blot analysis shows that ANXA2 expression is

significantly higher in injured kidney versus the control group. Mean±SEM.***P<0.001 Cisplatin versus Ctrl (n=5). (D) Immunofluorescent staining demonstrates that the upregulation of ANXA2 is observed across different sections of the injured kidney. White arrows indicate positive staining. Scale bars, 75 μm (low magnification); scale bars, 25 μm (high magnification). E F G Quantitative data show quantification of positive staining. Mean±SEM.**P<0.01,***P<0.001, Cisplatin (n=5) versus Ctrl group (n=5) (H) Co-localization of ANXA2 (red) with LTL (green, a marker for proximal renal tubule), PNA (green, a marker for distal renal tubule) and DBA (green, a marker for collecting duct) indicates ANXA2 is co-localized with proximal and distal renal tubules as well as with collecting ducts in injured kidney. White arrows indicate positive staining. scale bars, 25 μm. (I, J) Western blots shows urinary ANXA2 expression. Quantitative data was normalized by urine creatinine. Mean±SEM, ***P<0.001, Cisplatin (n=6) versus Ctrl (n=6). Abbreviations: ANXA2, annexin2; Ctrl, control.

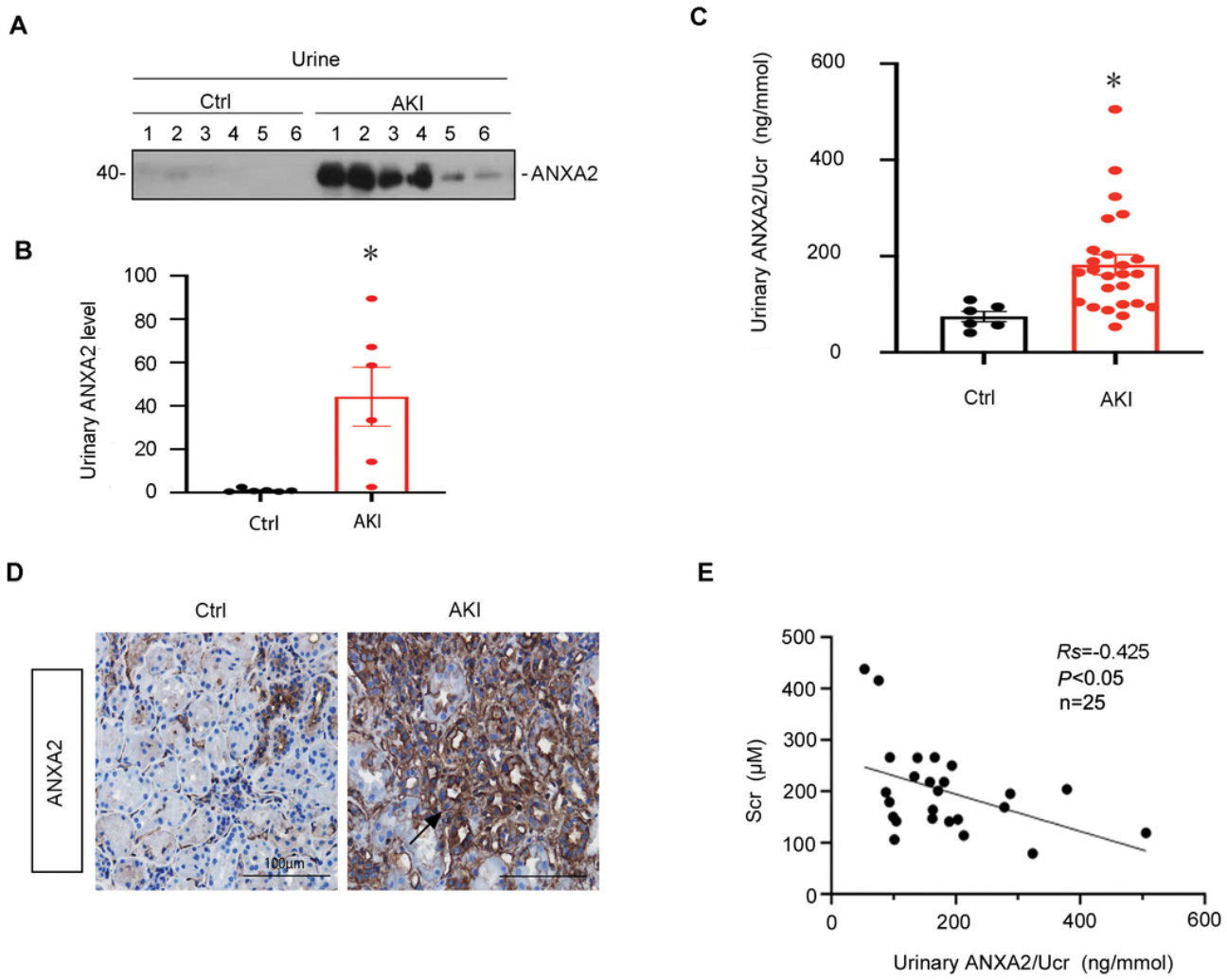

Figure 2

Figure 2

ANXA2 is upregulated in human AKI

(A B) Western blot demonstrates urine ANXA2 is higher in AKI patients than that in healthy donors. Quantitative data shows that urinary ANXA2 is significantly higher in AKI patients than in the healthy control. Quantification was normalized by Ucr. Mean±SEM, *P<0.05, AKI (n=6) versus Ctrl (n=6). (C) ELISA results demonstrate that urinary ANXA2 is significantly higher in AKI patients than in the healthy control. Mean±SEM, *P<0.05, AKI (n=25) versus Ctrl (n=6). (D) Immunohistochemical staining illustrates that ANXA2 expression is higher in the kidney sampled from AKI patients than the control participants. Black arrow indicates the positive staining. Scale bars, 100μm. (E) Scatter plot shows urinary ANXA2 versus serum creatinine reveals urine ANXA2 is negatively associated with serum creatinine. Rs=-0.425, P<0.05 n=25. Abbreviations: ANXA2, annexin2; Ctrl, control; Scr, serum creatinine; Ucr, urinary creatinine.

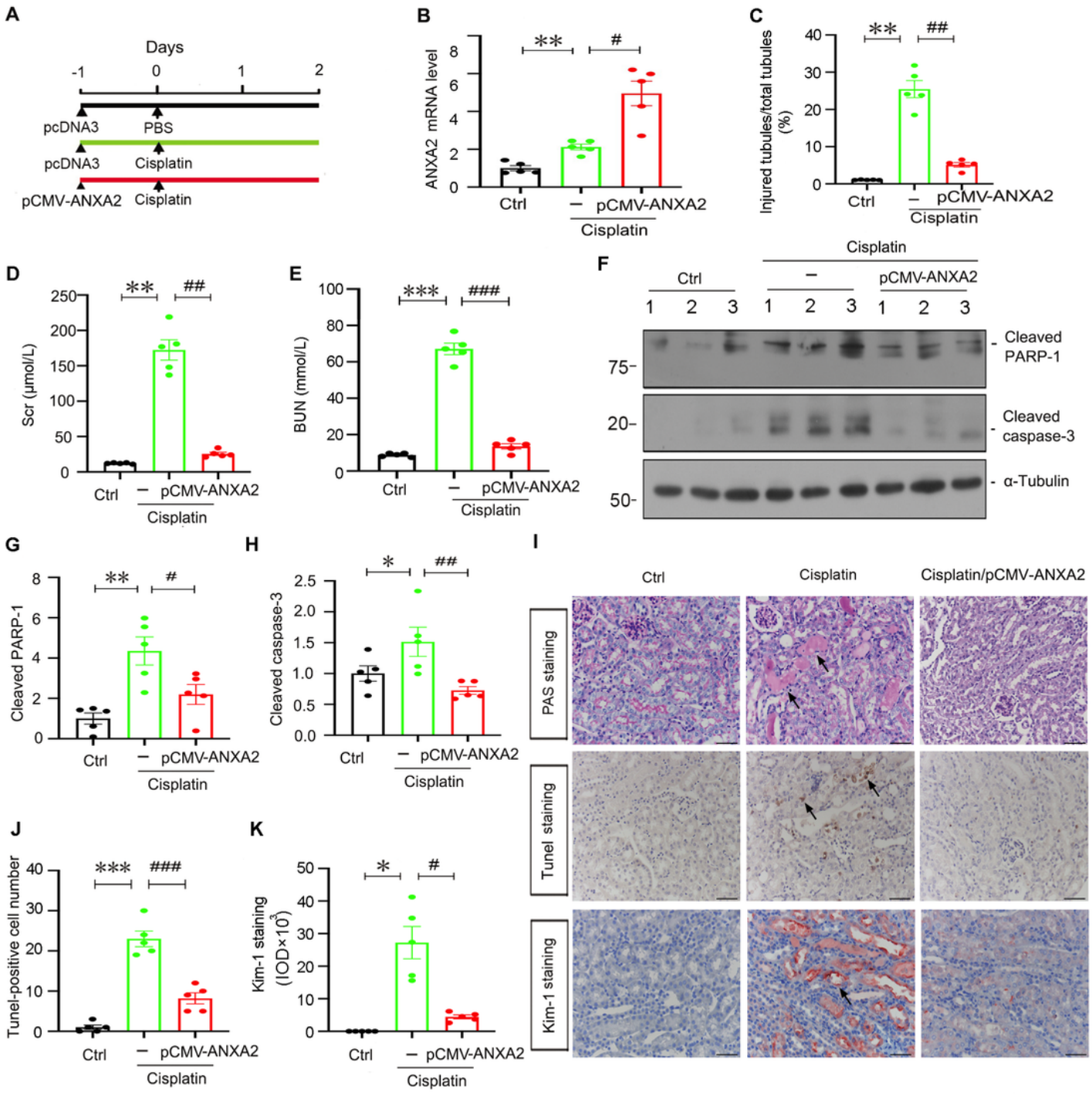

Figure 3

Figure 3

ANXA2 protects against AKI

(A) The schematic graph overviews the experimental design. (B) Quantitative data show that the plasmid injection induces the upregulation of ANXA2 gene expression. Mean±SEM,**P<0.01, pcDNA3+cisplatin(n=5) versus Ctrl(n=5); $^{\#}P$<0.05, cisplatin+pCMV-ANXA2 (n=5) versus

cisplatin+pcDNA3(n=5). (C) Quantitative data show that the ANXA2 overexpression plasmid injection decreases tubular injury. Mean±SEM. $^{**}P<0.01$, pcDNA3 +cisplatin(n=5) versus Ctrl (n=5); $^{\#\#}P<0.01$, cisplatin+pCMV-ANXA2 (n=5) versus cisplatin+pcDNA3 (n=5). (D, E) Scr and BUN assay demonstrates ANXA2 overexpression improves renal functions. Mean±SEM. $^{**}P<0.01$,$^{***}P<0.001$, pcDNA3+cisplatin (n=5) versus Ctrl (n=5); $^{\#\#}P<0.01$, $^{\#\#\#}P<0.001$, cisplatin+pCMV-ANXA2 (n=5) versus cisplatin+pcDNA3 (n=5). (F) Representative western blots and quantitative data show the expression of cleaved PARP (G) and caspase-3 (H), indicating ANXA2 overexpression alleviates apoptosis. Mean±SEM. *P<0.05, **P<0.01, pcDNA3+cisplatin(n=5) versus Ctrl(n=5); $^{\#}P<0.05$, ##P<0.01 cisplatin+pCMV-ANXA2 (n=5) versus cisplatin+pcDNA3 (n=5). (I) PAS staining of normal and injured kidney with or without ANXA2 overexpression demonstrates ANXA2 overexpression alleviates tubular injury. Black arrows indicate injured tubules. Scale bars, 50 μm. Tunel staining demonstrates ANXA2 overexpression alleviates apoptosis. Black arrows indicate apoptotic tubular cells which are colored brown. Scale bars, 50 μm. Kim-1 staining demonstrates ANXA2 overexpression alleviates tubular injury. The black arrow indicates the strong positive staining located in the brush border of tubular epithelial cells. Scale bars, 50 μm. (J K) Quantitative data show the number of TUNEL-positive tubular cells and positive staining of Kim-1. Mean±SEM. $^{*}P<0.05$, $^{***}P<0.001$, pcDNA3+cisplatin(n=5) versus Ctrl(n=5); $^{\#}P<0.05$, $^{\#\#\#}P<0.001$ cisplatin+pCMV-ANXA2 (n=5) versus cisplatin+pcDNA3 (n=5). Abbreviations: ANXA2, annexin A2; Ctrl, control; pcDNA3, empty vector pcDNA3

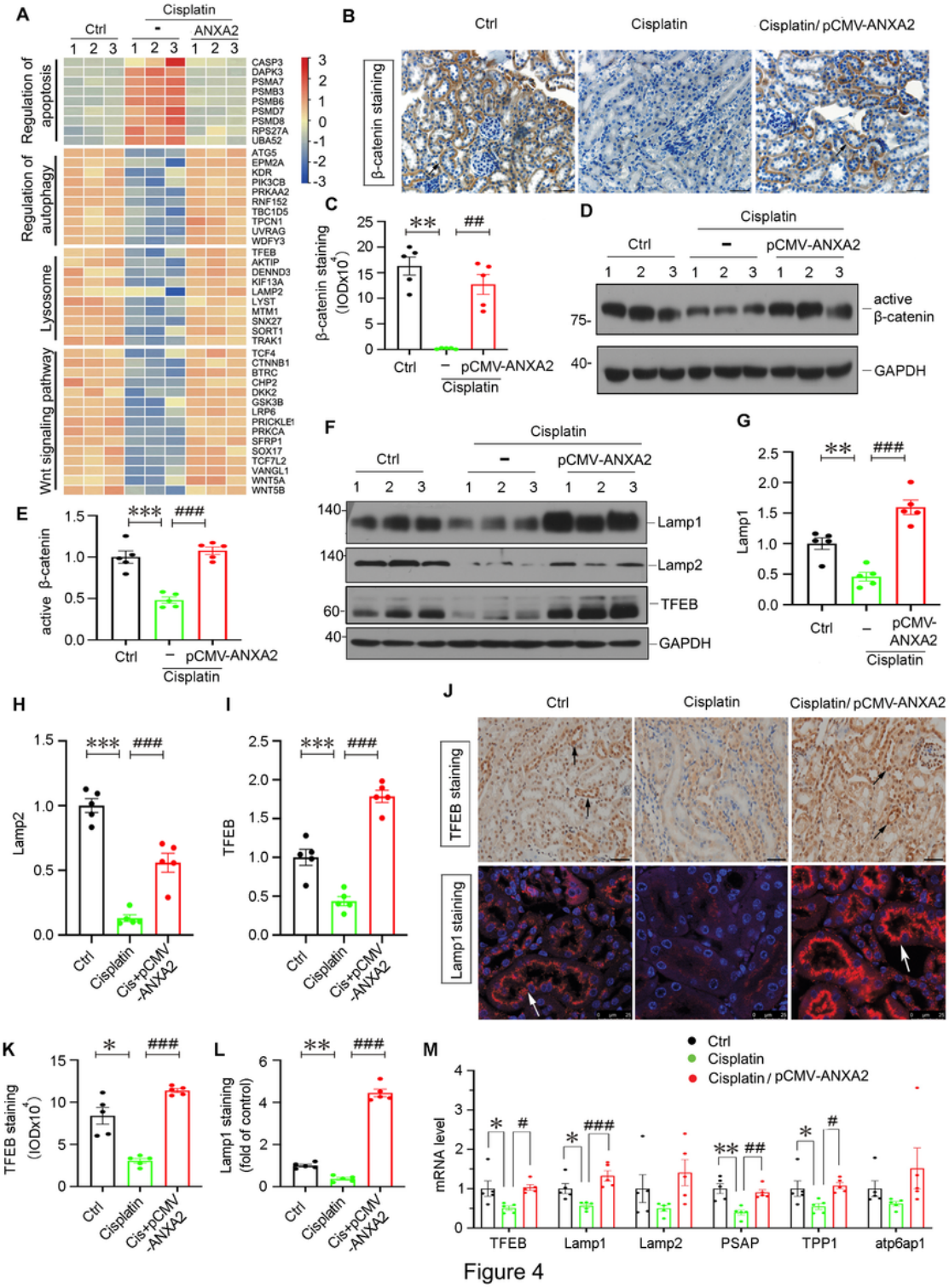

Figure 4

Figure 4

ANXA2 protects against AKI and this is associated with its regulatory effects on autophagy, lysosomal functions, and Wnt/β-catenin signaling

(A) Heatmap shows the FPKM value of genes sampled from different groups. Relevant genes are categorized into different GSEA gene sets. The color ranges from red to blue represents the log2 ranked

FPKM value from large to small. (B) Representative immunohistochemical staining of β-catenin in kidney tissues demonstrates ANXA2 overexpression restores the protein expression of β-catenin which is hampered by cisplatin. Black arrows indicate positive staining. Scale bars, 50 μm. C Quantitative data show quantification of positive staining. Mean±SEM.$^{**}P$<0.01, pcDNA3+cisplatin(n=5) versus Ctrl(n=5); $^{\#\#}P$<0.01 cisplatin+pCMV-ANXA2(n=5) versus cisplatin+pcDNA3(n=5). (D, E) Representative western blots (D) and quantitative data (E) show the induction of β-catenin in exposure to ANXA2 expression plasmid. Numbers (1 to 3) indicate individual animals in each group. Mean±SEM.$^{***}P$<0.001, pcDNA3+cisplatin(n=5) versus Ctrl(n=5); $^{\#\#\#}P$<0.001 cisplatin+pCMV-ANXA2(n=5) versus cisplatin+pcDNA3(n=5). (F to I) Representative western blots (F) and quantitative data (G to I) show the induction of Lamp1 (G), Lamp2 (H) and TFEB (I) by ANXA2 overexpression. Numbers (1 to 3) indicate individual animals in each group. Mean±SEM. $^{**}P$<0.01, $^{***}P$<0.001, pcDNA3+cisplatin (n=5) versus Ctrl (n=5) ; $^{\#\#\#}P$<0.001, cisplatin+pCMV-ANXA2 (n=5) versus cisplatin+pcDNA3 (n=5). (J) Representative immunostaining of TFEB (the top panel) and Lamp1 (the bottom panel) in kidney tissues demonstrates ANXA2 overexpression restores the protein expression of TFEB and Lamp1, which is hampered by cisplatin. Scale bars, 50μm and 25 μm. Arrows indicate positive staining of TFEB and Lamp1. (K L) Quantitative data show quantification of positive staining. Mean±SEM. $^{*}P$<0.05, $^{**}P$<0.01, pcDNA3+cisplatin (n=5) versus Ctrl (n=5); $^{\#\#\#}P$<0.001 cisplatin+pCMV-ANXA2 (n=5) versus cisplatin+pcDNA3 (n=5). (M) mRNA levels of TFEB, Lamp1, Lamp2, PSAP, TPP1 and Atp6ap1 in different groups demonstrate ANXA2 overexpression restores lysosomal functions. Mean±SEM, $^{*}P$<0.05, $^{**}P$<0.01, pcDNA3+cisplatin (n=5) versus Ctrl (n=5); $^{\#}P$<0.05, $^{\#\#}P$<0.01, $^{\#\#\#}P$<0.001 cisplatin+pCMV-ANXA2 (n=5) versus cisplatin+pcDNA3 (n=5) Abbreviations: ANXA2, annexin A2; Ctrl, control; FPKM, fragments per kilobase of transcript per million; GSEA, Gene Set Enrichment Analysis; pcDNA3, empty vector pcDNA.3.

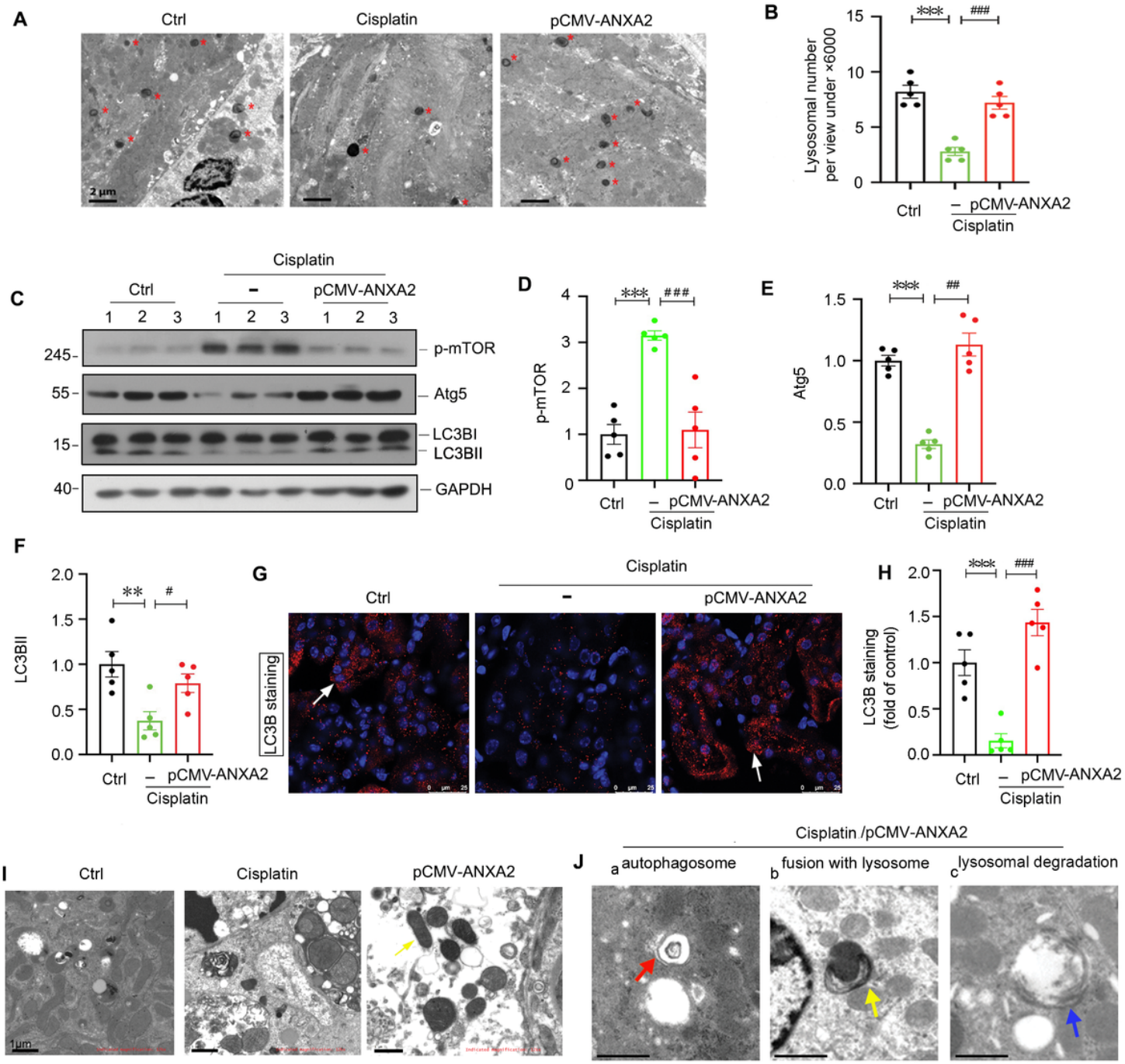

Figure 5

Figure 5

ANXA2 promotes lysosome-mediated autophagy function *in vivo*

(A) Transmission electron microscopy photos show the numbers of lysosomes (labeled by red stars) in renal tubular cells. The results demonstrate ANXA2 overexpression increases lysosomal numbers. Scale bars, 2 μm. (B) The lysosomal numbers were assessed and quantified under the view of 6000X magnification. Mean±SEM. ***P<0.001, pcDNA3+cisplatin (n=5) versus Ctrl(n=5); ###P<0.001, pCMV-

ANXA2+cisplatin(n=5) versus pcDNA3+cisplatin (n=5). (C to F) Representative western blots show the expression of p-mTOR (D), Atg5 (E) and LC3B (F). The results indicate ANXA2 overexpression promotes autophagy. Mean±SEM. **P<0.01, ***P<0.001, pcDNA3+cisplatin (n=5) versus Ctrl (n=5); $^{\#}$P<0.05, $^{\#\#}$P<0.01, $^{\#\#\#}$P<0.001 cisplatin+pCMV-ANXA2 (n=5) versus cisplatin+pcDNA3 (n=5). (G) Immunofluorescent staining of LC3B demonstrates autophagy is activated by ANXA2 overexpression. Scale bars, 25 μm. White arrows indicate LC3B puncta. (H) Quantitative data show quantification of positive staining. Mean±SEM. ***P*<0.001, pcDNA3+cisplatin (n=5) versus Ctrl (n=5); $^{\#\#\#}$*P*<0.001, pCMV-ANXA2+cisplatin (n=5) versus pcDNA3+cisplatin (n=5). (I) Transmission electron microscopy photos from proximal tubular cell reveal mitochondria were damaged by cisplatin but restored by ANXA2 overexpression. Yellow arrow indicates mitochondria. Scale bars, 1 μm. (J) Transmission electron microscopy from the mice of “Cisplatin/pCMV-ANXA2 group” indicate ANXA2 overexpression triggers a series of processes of autophagic flux. Red arrow, a double-membrane-shaped phagophore; Yellow arrow, an autophagosome which is bridging with a lysosome; Blue arrow, an autophagic vacuole undergoing degradation. Scale bars, 1 μm. Abbreviations: ANXA2, ANXA2; Ctrl, control; pcDNA3, empty vector pcDNA3.

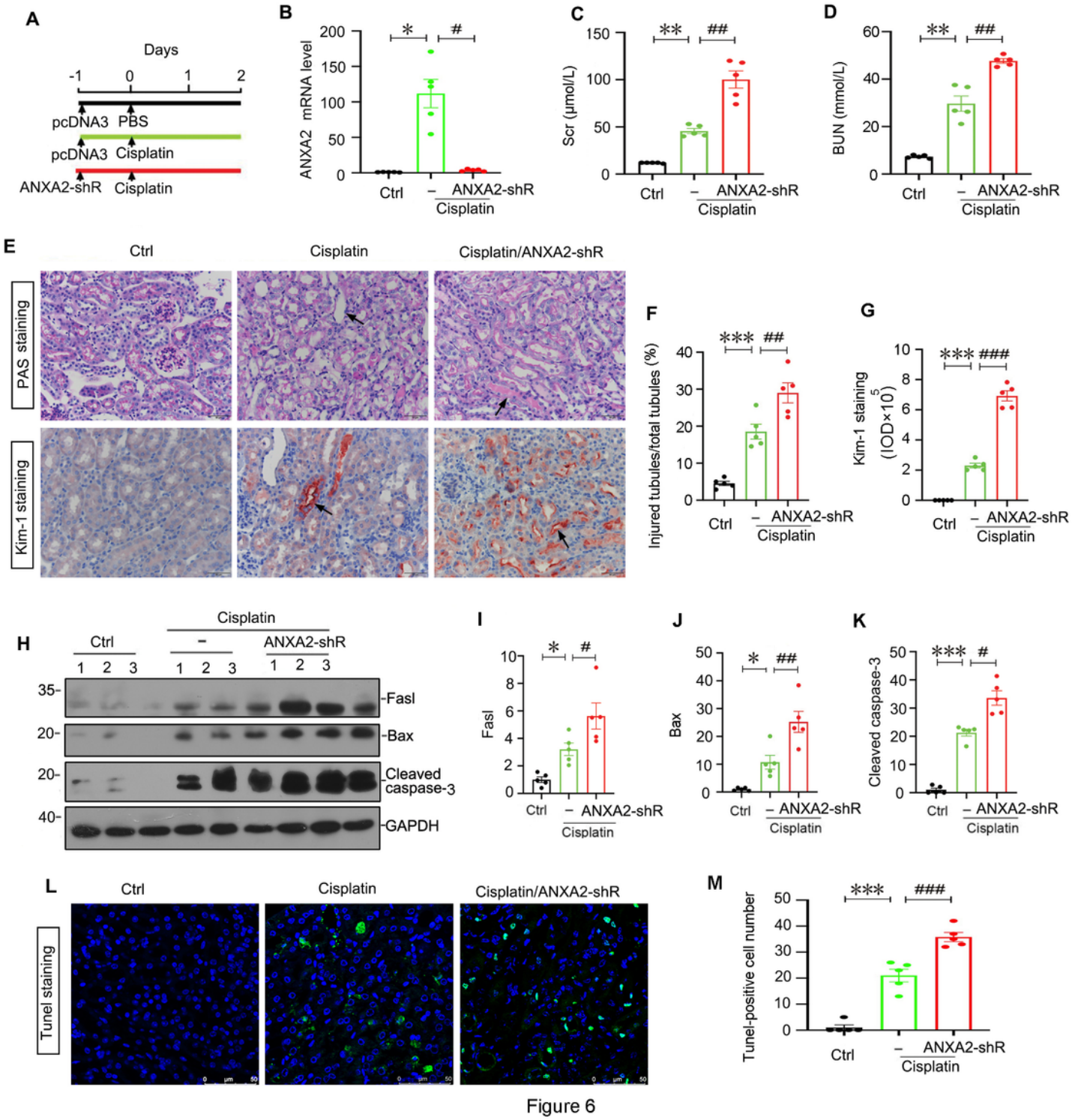

Figure 6

Figure 6

Knockdown of ANXA2 worsens AKI and apoptosis *in vivo*

(A) The schematic graph shows the experimental design. (B) The quantitative data show the plasmid injection induces knockdown of ANXA2 gene expression. Mean±SEM. **P*<0.05, pcDNA3+cisplatin (n=5) versus Ctrl (n=5); #*P*<0.05, shRNA-ANXA2+cisplatin (n=5) versus pcDNA3+cisplatin (n=5). (C, D) Scr (C)

and BUN (D) assay indicates knockdown of ANXA2 worsens renal functions. Mean±SEM. $^{**}P<0.01$, pcDNA3+cisplatin (n=5) versus Ctrl (n=5); $^{\#\#}P<0.01$, shRNA-ANXA2+cisplatin (n=5) versus pcDNA3+cisplatin (n=5). (E) Representative PAS staining (the top panel) demonstrates ANXA2 knockdown further worsens tubular injury in cisplatin-treated mice . Scale bars, 50mm. Black arrows indicate severely injured renal tubules with naked brush boarder; Representative Kim-1 staining (the bottom panel) demonstrates ANXA2 knock-down worsens tubular injury caused by cisplatin. Scale bars, 50mm. Black arrows indicate injured renal tubules. (F G) Quantitative data show quantification of positive staining. Mean±SEM. $^{***}P<0.001$, pcDNA3+cisplatin (n=5) versus Ctrl (n=5); $^{\#\#}P<0.01$, $^{\#\#\#}P<0.001$ shRNA-ANXA2+cisplatin (n=5) versus pcDNA3+cisplatin (n=5). (H to K) Representative western blots (H) show the expression of Fasl (I), Bax (J) and cleaved caspase 3 (K) The results indicate knockdown ANXA2 expression induces apoptosis. Mean±SEM. $^{*}P<0.05$ $^{***}P<0.001$, pcDNA3+cisplatin (n=5) versus Ctrl (n=5); $^{\#}P<0.05$, $^{\#\#}P<0.01$ shRNA-ANXA2+cisplatin (n=5) versus pcDNA3+cisplatin (n=5). (L) Representative photos indicate knockdown ANXA2 expression increases TUNEL-positive apoptotic cells. Scale bars, 50 μm. M Quantitative data show quantification of positive staining. Mean±SEM. $^{***}P<0.001$, pcDNA3+cisplatin (n=5) versus Ctrl (n=5); $^{\#\#\#}P<0.001$ shRNA-ANXA2+cisplatin (n=5) versus pcDNA3+cisplatin (n=5). Abbreviations: ANXA2, annexin A2; Ctrl, control; pcDNA3, empty vector pcDNA3; shRNA, small hairpin RNA.

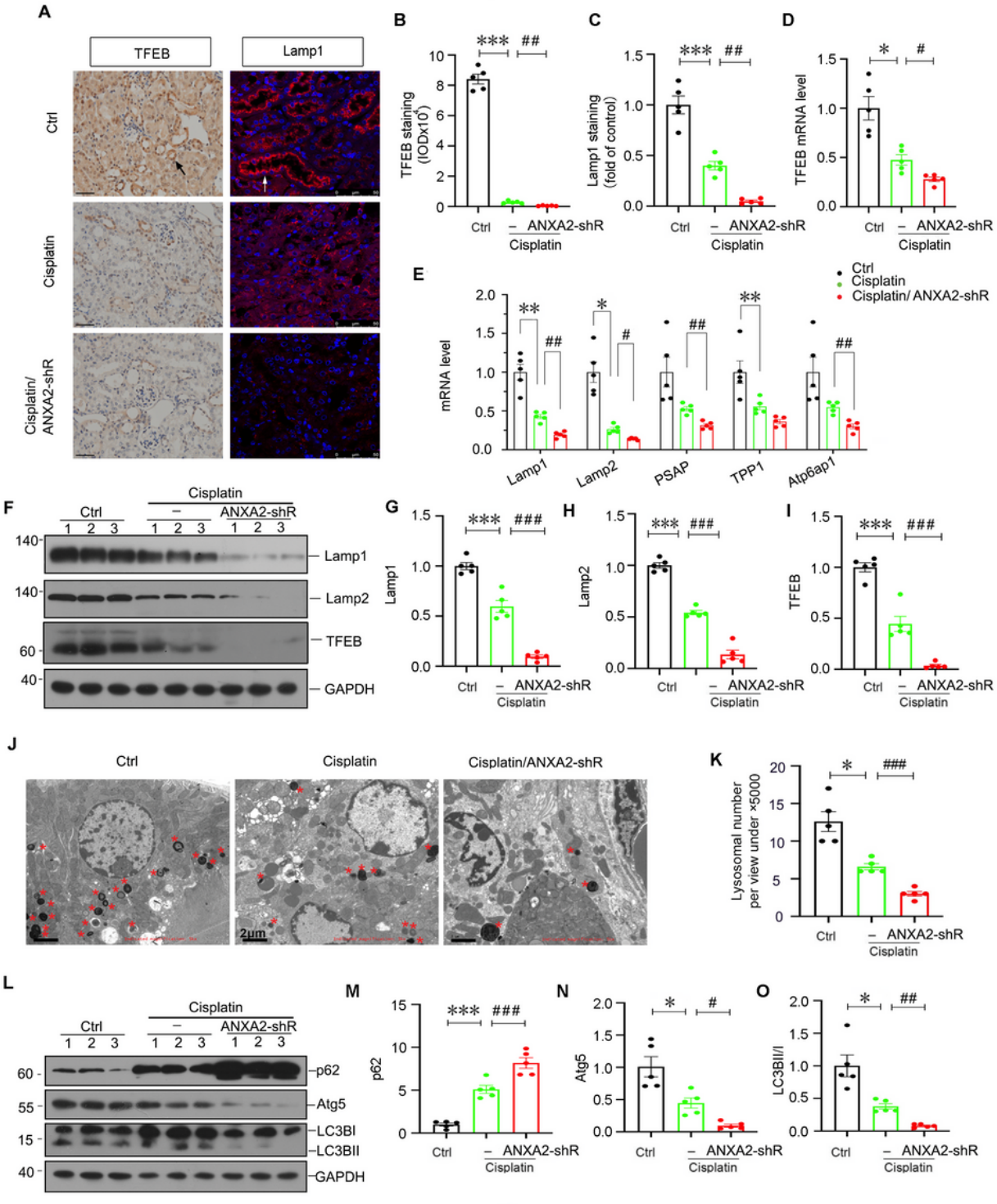

Figure 7

Figure 7

Knockdown of ANXA2 decreases lysosomal function and inhibited autophagy

(A) Representative immuno-staining of TFEB (the left panel) and Lamp1 (the right panel) in kidney tissues demonstrates ANXA2 knockdown further inhibited the protein expression of TFEB and Lamp1. Scale bars, 50 μm. Arrows indicate positive staining. (B C) Quantitative data show quantification of

positive staining. Mean±SEM. ***P<0.001, pcDNA3+cisplatin (n=5) versus Ctrl (n=5); $^{\#\#}P$<0.01 shRNA-ANXA2+cisplatin (n=5) versus pcDNA3+cisplatin (n=5). (D E) mRNA assay of TFEB, Lamp1, Lamp2, PSAP, TPP1 and Atp6ap1 demonstrates ANXA2 knockdown further worsens lysosomal functions in cisplatin. Mean±SEM, *P<0.05 **P<0.01, pcDNA3+cisplatin (n=5) versus Ctrl (n=5); $^{\#}P$<0.05 $^{\#\#}P$<0.01 shRNA-ANXA2+cisplatin (n=5) versus pcDNA3+cisplatin (n=5). (F to I) Representative western blots (F) show the expression of Lamp1 (G), Lamp2 (H) and TFEB (I). The results indicate ANXA2 knockdown inhibits lysosomal functions. Mean±SEM. ***P<0.001, pcDNA3+cisplatin (n=5) versus Ctrl (n=5); $^{\#\#\#}P$<0.001, shRNA-ANXA2+cisplatin (n=5) versus pcDNA3+cisplatin (n=5). (J) Transmission electron microscopy photos demonstrate ANXA2 knockdown decreases number of lysosomes (labeled by red stars) in proximal renal tubular cells. Scale bars, 2 μm. (K) The lysosomal number was assessed and quantified under the view of 5000X magnification. Mean±SEM. *P<0.05, pcDNA3+cisplatin (n=5) versus Ctrl (n=5); $^{\#\#\#}P$<0.001, ANXA2-shR+cisplatin (n=5) versus pcDNA3+cisplatin (n=5). (L to O) Representative western blots (L) show the expression of p62 (M), Atg5 (N) and LC3BII/I (O) The results indicate ANXA2 knockdown inhibited autophagy. Mean±SEM. *P<0.05, ***P<0.001, pcDNA3+cisplatin (n=5) versus Ctrl (n=5); $^{\#}P$<0.05 $^{\#\#}P$<0.01 $^{\#\#\#}P$<0.001, shRNA-ANXA2+cisplatin (n=5) versus pcDNA3+cisplatin (n=5). Abbreviations: ANXA2, annexin A2; Ctrl, control; pcDNA3, empty vector pcDNA3; shRNA, small hairpin RNA.

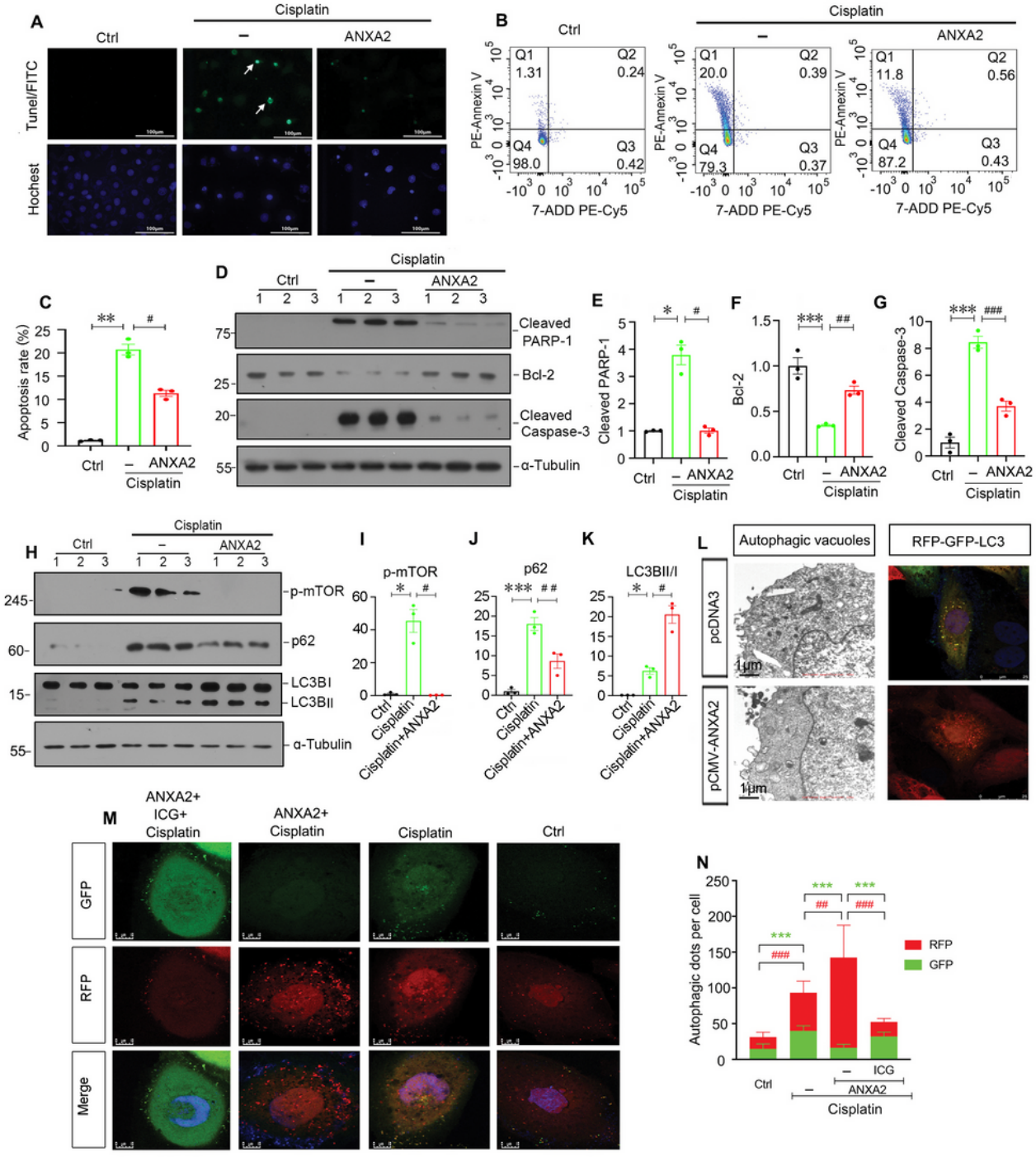

Figure 8

Figure 8

ANXA2 blocks renal tubular cell apoptosis and promotes autophagy *in vitro*

HK-2 cells were stimulated by cisplatin (25 μg/mL) for 24 hour's with or without a previous 24 hour-pretreatment of recombinant human ANXA2 protein (2 μg/mL). (A) Representative TUNEL staining shows the number of apoptotic HK-2 cells (green fluorescence) *in vitro*. Scale bars, 100 μm. (B, C) Flow

cytometry analysis showing the ratio of apoptotic cells (annexin V5 positive/7-ADD negative) *in vitro*. Mean±SEM. $^{**}P<0.01$, Cisplatin (n=3) versus Ctrl (n=3); $^{\#}P<0.05$, ANXA2+Cisplatin (n=3) versus Cisplatin (n=3). (D-G) Representative western blots and quantitative data showing the expression of cleaved PARP-1 (E), Bcl2 (F) and cleaved caspase-3 (G) in different groups as indicated. The results demonstrate ANXA2 inhibited the apoptosis in HK-2 cells. Mean±SEM. $^{*}P<0.05$ $^{***}P<0.001$, Cisplatin alone (n=3) versus Ctrl (n=3); $^{\#}P<0.05$ $^{\#\#}P<0.01$, $^{\#\#\#}P<0.001$, ANXA2+Cisplatin (n=3) versus Cisplatin only (n=3). (H-K) Representative western blots (H) show the expression of p-mTOR (I), p62 (J) and LC3B (K) in different groups as indicated. Mean±SEM. $^{*}P<0.05$, $^{***}P<0.001$, Cisplatin only (n=3) versus Ctrl (n=3); $^{\#}P<0.05$, $^{\#\#}P<0.01$ ANXA2+Cisplatin (n=3) versus Cisplatin only (n=3). (L) Transmission electron microscopy clearly demonstrates that ANXA2 expression plasmid transfection increases the numbers of autophagic vacuoles (left panel). Scale bars, 1 μm.; ANXA2 overexpression increases lysosomal functions as evidenced by enhanced RFP (red) LC3B positive puncta being captured in ANXA2 expression plasmid transfected HK-2 cells (right panel). Scale bars, 25 μm. (M) ANXA2 promotes the autophagic flux in HK-2 cells. HK-2 cells were transiently transfected with RFP-GFP-LC3B lentivirus for 24 hours before treatment with ANXA2 recombinant protein (2 μg/mL), or ANXA2 with cisplatin (25 μg/mL) or ANXA2 with cisplatin and ICG-001 (10μM). Red fluorescence, acidic-pH, and LC3B-positive autolysosomes; Green fluorescence, neutral-pH LC3B-positive autophagosomes. Scale bars, 10 μm. (N) Numbers of autophagosomes (green fluorescence) and autolysosomes (red fluorescence) were counted in randomly selected 10 cells for each group. Quantitative data of autophagosomes (green) and autolysosomes (red) are shown in the bar graph. Mean±SEM. $^{***}P<0.001$, $^{\#\#}P<0.01$, $^{\#\#\#}P<0.001$. The comparisons between every groups are available as labelled. (n=10). Abbreviations: ANXA2, annexin A2; Ctrl, control; ICG, ICG-001; pcDNA3, empty vector pcDNA3; TUNEL, terminal deoxynucleotidyl transferase dUTP nick-end labeling.

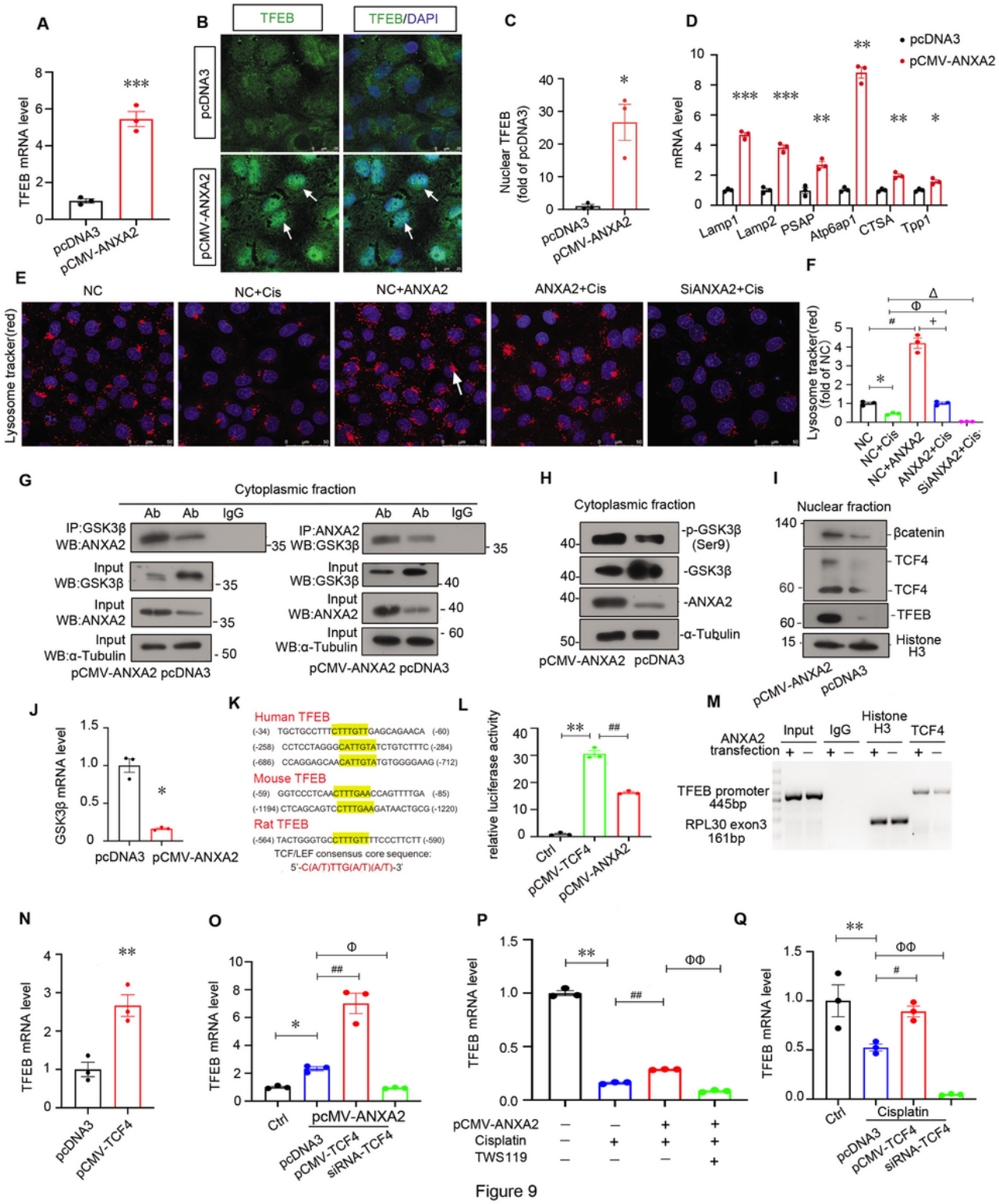

Figure 9

Figure 9

ANXA2 promotes lysosomal functions through β-catenin/TCF4 signaling

(A, D) HK-2 cells were transfected with ANXA2 expression plasmid for 24 hours. mRNA assay of TFEB indicates ANXA2 overexpression promotes lysosomal functions. Mean±SEM. *P<0.05, **P<0.01,***P<0.001, pCMV-ANXA2 (n=3) versus pcDNA3 (n=3). (B C) Representative photos show the

immunofluorescent staining of TFEB *in vitro*. Scale bars, 25 μm. White arrows indicate staining of TFEB in nuclear area. Quantitative data show quantification of positive staining. Mean±SEM. **P*<0.05, pCMV-ANXA2 (n=3) versus pcDNA3 (n=3). (E) HK-2 cells were grown on confocal dishes for microscopy. Either human recombinant ANXA2 protein (2 μg/mL) or ANXA2 small interfering RNA (siRNA, 100nM) was applied to HK-2 cells, after which cisplatin (25 μg/mL) was added for 24h. Lysosomal tracker staining assay shows different intensities of lysosome fluorescence. The white arrow indicates positive staining. Scale bars, 50 μm. F Quantitative data show quantification of positive staining. Mean±SEM. **P*<0.05, cisplatin (n=3) versus NC (n=3); $^{\#}$*P*<0.05, ANXA2 (n=3) versus NC (n=3); $^{+}$P<0.05 cisplatin+ANXA2 (n=3) versus ANXA2 (n=3);$^{\varphi}$P<0.05 cisplatin+ANXA2 (n=3) versus cisplatin (n=3); P<0.05 cisplatin+siANXA2 (n=3) versus cisplatin(n=3); (G) Co-IP analysis reveals the binding activities of ANXA2 with GSK3β. (H, I) Western blotting showing protein levels of β-catenin, GSK3β, ANXA2 and TCF4 in the nucleus and cytosol fractions HK-2 cells were transfected with either the ANXA2 overexpression plasmid or the empty vector for 24h. (J) mRNA assay indicates ANXA2 overexpression downregulated GSK3β expression. Mean±SEM. **P*<0.05, pCMV-ANXA2 (n=3) versus pcDNA3 (n=3). (K) Bioinformatic assay shows predicted potential binding sites of TCF4 in TFEB promoter region. The consensus binding sequence could be detected in human, mouse, and rat. (L) HK-2 cells were transiently co-transfected with 0.1μg of renilla luciferase, 1ug of pGL3-TFEB promoter reporter plasmid, and 1ug of ANXA2 or TCF4 overexpression plasmid. The activity of TFEB transcription is determined by dual-luciferase assays. Data are presented as the relative ratio of renilla luciferase activity and firefly luciferase activity. Mean±SEM. ***P*<0.01, pCMV-TCF4 (n=3) versus ctrl (n=3); $^{\#\#}$*P*<0.01, pCMV-ANXA2 (n=3) versus pCMV-TCF4 (n=3). (M) The higher TFEB transcriptional activity was detected in ANXA2 overexpression group using ChIP-PCR analysis. (N) mRNA assay indicates TCF4 overexpression promotes TFEB expression. Mean±SEM. ***P*<0.01, pCMV-TCF4 (n=3) versus pcDNA3 (n=3). (O) Quantitative data show the mRNA level of TFEB in different group. Mean±SEM. **P*<0.05, pCMV-ANXA2 (n=3) versus ctrl (n=3); $^{\#\#}$*P*<0.01, pCMV-ANXA2+pCMV-TCF4 (n=3) versus pCMV-ANXA2 (n=3). $^{\varphi}$*P*<0.05, pCMV-ANXA2+siRNA-TCF4 (n=3) versus pCMV-ANXA2 (n=3) .(P) HK-2 cells were transfected with ANXA2 expression plasmid and/or exposed to TWS119 (1μM) for 24 hours before being treated by cisplatin (25μg/mL) for another 24h. Quantitative data show the mRNA levels of TFEB in different group. Mean±SEM. ***P*<0.01, cisplatin(n=3) versus ctrl (n=3); $^{\#\#}$*P*<0.01, cisplatin+pCMV-ANXA2 (n=3) versus cisplatin (n=3).$^{\varphi\varphi}$*P*<0.01, cisplatin+pCMV-ANXA2+TWS119 (n=3) versus cisplatin+pCMV-ANXA2 (n=3). (Q) Quantitative data show the mRNA levels of TFEB in different group.HK-2 cells were transfected with TCF4 expression plasmid or siRNA, and then treated with cisplatin for 24h. Mean±SEM. ***P*<0.01, cisplatin+pcDNA3 (n=3) versus ctrl (n=3); $^{\#}$*P*<0.05, cisplatin+pCMV -TCF4 (n=3) versus cisplatin+pcDNA3 (n=3). $^{\varphi\varphi}$*P*<0.01, cisplatin+siRNA-TCF4 (n=3) versus cisplatin+pcDNA3 (n=3). Abbreviations: Ab, antibody; ANXA2, ANXA2 ChIP, chromatin immunoprecipitation; Ctrl, control; Ctnnb1, catenin beta 1; GSK3β, glycogen synthase kinase 3; Lamp1, lysosomal associated membrane protein 1; TCF4, T-cell factor 4; TFEB, transcription factor EP; TPP1, tripeptidyl peptidase 1; pcDNA3, empty vector pcDNA3.

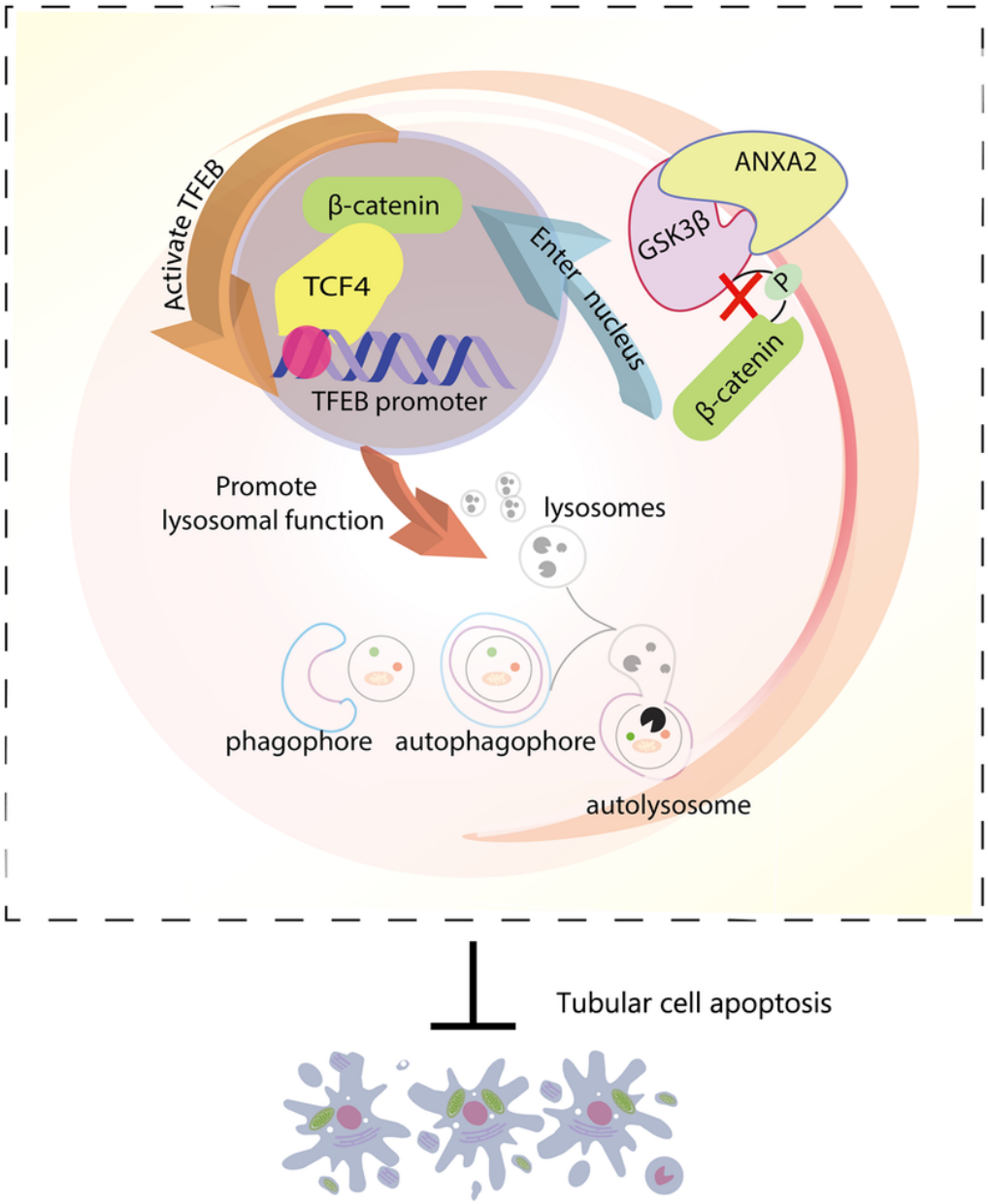

Figure 10

Figure 10

Working model

Cellular machinery model graph illustrates that ANXA2 plays a key role in lysosomal functions through GSK3β/β-catenin/TFEB pathway. Specifically, ANXA2 binds to GSK3β, thereby blocking the activity of GSK3β. This leads to β-catenin to enter into the nucleus to trigger TCF4-induced TFEB transcription.

Consequently, lysosome biogenesis and lysosome-mediated autophagic flux are promoted to inhibit cell apoptosis in renal tubular cells. This provides a new potential therapeutic target for AKI.

Supplementary Files

This is a list of supplementary files associated with this preprint. Click to download.

- ajchecklist.pdf
- SupplementaryData.docx